https://doi.org/10.5194/egusphere-2026-3939
Preprint. Discussion started: 12 August 2026

Impact of meteorological conditions on rockfalls: a case study of the Saint Eynard cliff

Sabrine Bouaziz[1], David Amitrano[2], Christophe Lin-Kwong-Chon[1], Nicolas Méger[1], and Agnès Helmstetter[2]

[1]*Université Savoie Mont Blanc, Polytech Annecy-Chambéry, LISTIC, Annecy, France*
[2]*Univ. Grenoble Alpes, Univ. Savoie Mont Blanc, CNRS, IRD, Univ. Gustave Eiffel, ISTerre, 38000 Grenoble, France*

Correspondence: Sabrine Bouaziz (sabrine.bouaziz@univ-smb.fr), David Amitrano (david.amitrano@univ-grenoble-alpes.fr), Christophe Lin-Kwong-Chon (christophe.lin-kwong-chon@univ-smb.fr), Nicolas Méger (nicolas.meger@univ-smb.fr), and Agnès Helmstetter (agnes.helmstetter@univ-grenoble-alpes.fr)

Abstract. Rockfall events are influenced by various climatic factors. Identifying these factors is crucial for anticipating rockfall events and managing the risks to infrastructure and populations. Previous studies have particularly highlighted rainfall and freezing conditions as key triggers, based on rockfall catalogs derived from visual observations or diachronic comparisons, with temporal precision ranging from a few to several days.

The purpose of this study is to use a catalog derived from seismic detection, which provides much greater temporal accuracy, to explore and better understand the meteorological conditions that contribute to rockfalls at Mont Saint-Eynard, a limestone cliff in the French Alps. This study introduces a probabilistic approach that combines different temporal horizons and cumulative models capturing delayed effects to analyze the influence of rainfall and freezing conditions on rockfall triggering. By integrating multiple statistical metrics related to specific meteorological conditions including empirical probabilities, lift measures, confidence intervals and Chi-squared tests, we identify not only the likelihood but also the strength and reliability of triggering patterns. Our results highlight the significant role the significant role of short-term triggers like recent intense rainfall on high magnitude rockfall, and the delayed effect of freezing depth in rockfall activity. This knowledge could be used to implement a risk management strategy.

1 Introduction

Rockfalls pose a major risk to infrastructure and public safety, particularly in mountainous areas. This phenomenon can cause significant material damage, road closures, and high economic costs. They are often triggered by meteorological factors such as intense rainfall and temperature variations, which influence mechanical loading and weakening processes through water infiltration and freeze–thaw cycles. As a result, rockfall activity reveals strong temporal variability with periods of increased occurrence are often associated with specific meteorological conditions.

Several studies have been conducted to understand the relationship between rockfalls and meteorological factors. The main difference between these studies is the level of detail in the rockfall catalogs, in terms of both volume and time resolution. Some studies are based on direct observation of the rockfall impacts on infrastructure (Rat (2006),Chanut et al. (2021),Delonca et al.

https://doi.org/10.5194/egusphere-2026-3939
Preprint. Discussion started: 12 August 2026

(2014) with poor details on volume and temporal resolution of approximately one day. Other studies are based on diachronic comparison of point clouds obtained by Lidar or Photogrammetry (e.g. D'Amato et al. (2016)) providing accurate estimates of rockfall volume associated with temporal resolutions of several days to months depending on the survey frequency. The use of seismic monitoring for rockfall detection allows to reach temporal precision of seconds (Helmstetter and Garambois (2010); Le Roy et al. (2019)) but the estimation of the volume requires to establish a relationship with seismic signal features that appear complex and then relatively imprecise (Le Roy et al. (2019)) compared to point-cloud-based methods.

A study comparing three different sites located in France (La Réunion, Bourgogne, and Auvergne) by Delonca et al. (2014) further illustrated the variability of meteorological influences on rockfalls across regions. At La Réunion, heavy rainfall between 15–20 mm with a cumulative effect over two days, is strongly correlated with rockfalls, which often occur within a day after the rainfall with an empirical daily rockfall probability of 0.32. This probability rises to 0.55 for rainfall between 40–50 mm. This represented a considerable probability increase when compared to the annual average daily rockfall probability of 0.13. In Burgundy, the daily rockfall probability increases from 0.02 to 0.04 under 15–20 mm cumulative rainfall over three days, with events often occurring two days after the rainfall. Meanwhile, in Auvergne, freeze-thaw cycles, especially minimal temperatures below 0°C, are the most significant triggering factors, where the probability of rockfall increases from 0.029 globally to 0.039 when minimum temperatures fall between –5°C and 0°C, with rockfalls delayed by 2 days following the freezing event.

Additionally, a study on the Route du Littoral in La Réunion emphasizes the role of rainfall in managing rockfall risks on basaltic cliffs Rat (2006). In 2004, an initial management rule stated that the road should remain closed for three days if rainfall exceeded 30 mm in 24 hours. With more precise rockfall monitoring, these thresholds were adjusted Chanut et al. (2024). By 2009, the road would be closed for one day if rainfall ranged between 40 and 50 mm and for two days if it exceeded 50 mm in 24 hours.

D'Amato et al. (2016) thesis explores the impact of weather conditions, particularly rainfall events and freeze-thaw cycles, on rockfalls occurred at the Saint-Eynard limestone cliff. The results show that rockfall frequency can increase by up to a factor of seven during freeze-thaw cycles and by a factor of 26 when the average rainfall intensity (since the onset of rainfall) exceeds 5 mm/h. As the authors based the detection of rockfalls on four LiDAR surveys spreading over 2.5 years and associated with photos taken every 2 to 11 weeks, the meteorological effects they established can be considered as averaged over several weeks.

Using seismological detection of rockfalls Helmstetter and Garambois (2010) were able to report such relationship at a shorter time scale of several hours for the case study of Séchilienne rockslide (France). They highlighted a weak but significant correlation between rockfall occurrences and rainfall intensity, with a linear increase in rockfall frequency as precipitation intensity increased. This work revealed the absence of a specific rainfall threshold for triggering rockfall events, showing that even light rainfall (1 mm) could be enough to trigger rockfalls. It is also observed that rockfall activity began almost immediately during a rainfall episode and can persist for several days after the rainfall ends. It should be noted that in this case, the rockfalls originate from an unstable rocky slope and not from a cliff per se. The rainfall also had a notable impact on the deformation of the whole rockslide.

https://doi.org/10.5194/egusphere-2026-3939
Preprint. Discussion started: 12 August 2026

Such correlations have been also observed in various countries and geological (Birien and Gauthier, 2023; Nissen et al., 2022; Krautblatter and Moser, 2009).

The state of the art highlights the significant influence of rainfall and sub-zero temperatures on rockfall events. While correlations have been established between rainfall and rockfall occurrence, the precise understanding of the underlying mechanisms remains limited, particularly regarding the absence of specific rainfall thresholds for triggering rockfalls or the variability in the timing of post-rainfall activity. These findings have primarily relied on expert interpretation. Thus, it is essential to deepen the analysis of data to identify the specific meteorological conditions under which rockfall risks are highest.

In most studies, rockfall detection is performed by road maintenance personnel with a temporal resolution of one day, with poor precision for the volume estimation due to visual detection. When using LiDAR surveys the precision of rockfall volume estimation is increased but the temporal resolution is significantly decreased. In both cases temporal resolution can limit the ability to precisely link rockfall events to specific meteorological triggers.

In the present study, our main objective is to improve the understanding of rockfall triggering factors at Mont Saint-Eynard. To achieve this, we combine high-resolution meteorological data with continuous seismic monitoring, allowing for the detection of rockfalls with greater temporal accuracy. This approach aims to identify the specific conditions that increase the probability of rockfall occurrence.

2 Study site and data

This study focuses on the Mont Saint-Eynard site, located near the town of Grenoble (Figure **??** and Figure **??**). It is a limestone cliff in the Chartreuse massif that rises to an altitude of 1,379 m and stretches over a length of 5 km. This site experiences frequent rockfall events, with nearly daily occurrences. Several towns, such as Biviers, Corenc, Meylan, Saint Ismier, and Saint Nazaire Les Eymes, lie at the base of the cliff, making this densely populated area(approximately 800 inhabitants km^2) particularly vulnerable to rockfall hazards. The overall morphology of Mont Saint-Eynard consists of two subvertical cliffs. The lower cliff of Sequanian stage, is 240 m high on average and consists of fractured thin-bedded limestone prone to rockfall. It is separated from the upper cliff by a 120 m high forested ledge. The upper cliff consists of massive limestone of the Tithonian stage, in which the rockfall activity is lower. The lower cliff exhibits an activity level 22 times higher in terms of rockfall occurrences compared to the upper cliff D'Amato (2017). The rockfall activity was first determined through a study conducted by Guerin et al. (2014) using terrestrial laser scanning over a 3-year period. This study detected 344 rockfall events exceeding 0.05 m^3 during this time on a surveyed surface located at the southern limit of the cliff (about 1 km in length and 200 m high), demonstrating the ongoing activity of these rock instabilities. Since 2013, this site has been subject to continuous seismic monitoring, aimed at systematically detecting rockfall events. More details about the seismic network and the methodology for identifying the signal produced by rockfall can be found in Le Roy et al. (2019); Provost et al. (2018).

This study proposes a uniform methodology for quantifying the influence of meteorological conditions on rockfall occurrence, by introducing an empirical conditional-probability-based framework calculated over retrospective (RH) and forecast (FH) horizons:

https://doi.org/10.5194/egusphere-2026-3939
Preprint. Discussion started: 12 August 2026

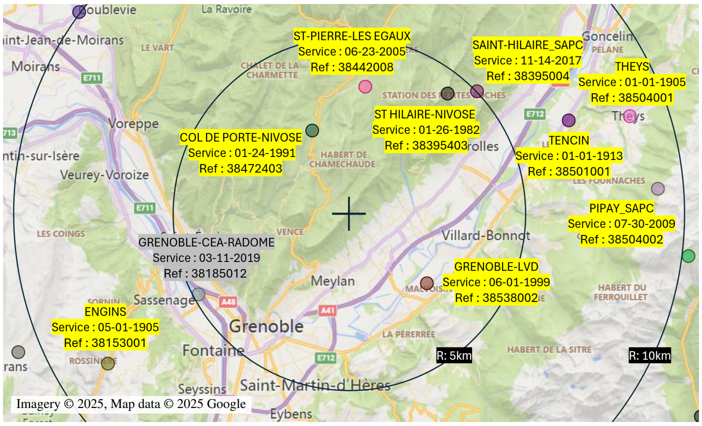

(a) Location of the study site within France. Imagery © 2025, Map data © 2025 Google.

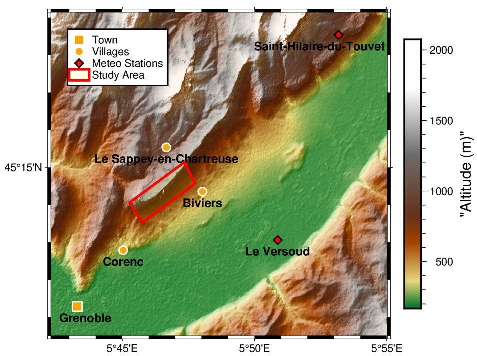

(b) Study area and meteorological stations used in this study.

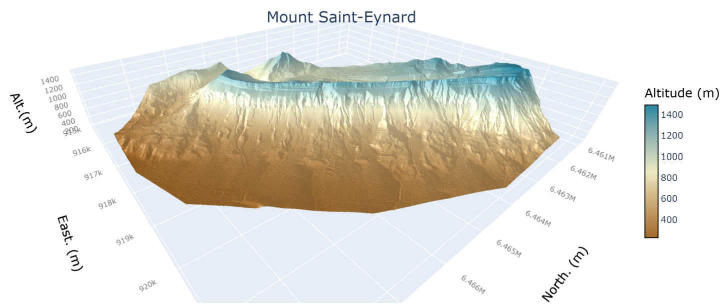

(c) 3D view of the Saint-Eynard cliff.

Figure 1. Location and overview of the study site.

– For continuous rainfall conditions, our results show that rainfall accumulated over short retrospective horizons ($1 < RH < 4$) significantly increases rockfall probability regardless of the forecast horizon.

– Using threshold-based conditioning, we find that combinations of low rainfall–small rockfall and large rainfall-large rockfall contribute more strongly to rockfall occurrence over short and long forecast horizons (FH) respectively, than cross-combinations.

– The rainfall charge/discharge analysis reveals that high levels of accumulated hydrological charge are associated with the highest increases in rockfall occurrence.

– For freezing conditions, continuous negative temperatures show an increase in rockfall probability across all forecast horizons (FH) with the strongest influence for retrospective horizons between 1 and 7 days.

https://doi.org/10.5194/egusphere-2026-3939
Preprint. Discussion started: 12 August 2026

– The freezing-depth indicator shows that greater freezing depths are associated with elevated rockfall likelihood.

This work provides a detailed and quantitative analysis of how meteorological conditions act across different temporal horizons to influence rockfall occurrence.

2.1 Data description

In this section, we present and analyze the datasets used in the study. These consist of a seismic event catalog, as well as precipitation and temperature measurements, collected over nearly ten years (2013–2024). We begin by describing the distributions of each dataset at hourly, daily, and monthly resolutions. We then examine the conditional distributions by comparing periods with rockfall activity to the entire observation period to estimate the ratio between the conditional empirical probability (during rockfall periods) and the baseline empirical probability (over the full period).

2.1.1 Time Series of Seismic Events

The seismic event time series is an event-based dataset obtained using a standard detection algorithm (short-time average window (STA)/ long-time average window (LTA), Allen (1978); Le Roy et al. (2019)). The seismic sensors used are velocimeters, i.e. the signal amplitude scales with the ground velocity [nm/s].

Each record in this catalog includes the following attributes:

- Detection time,
- Maximum amplitude of the signal [nm/s], averaged over all seismic stations,
- "pseudo-energy" generated by the event, defined as the integral of the squared signal amplitude over the event duration averaged over all seismic stations [$(\mathrm{nm/s})^2$]
- Duration of the signal [s],
- Average frequency of the seismic signal [Hz],
- Event type, categorized as one of the following:
  - S: Seismic event
  - R: Rockfall event
  - N: Noise

For the purpose of this study, we focus exclusively on the attributes detection time, event type, and amplitude because they are the most consistent as they allow us to link each event to meteorological conditions, assess its occurrence timing, and evaluate its potential intensity. Previous studies (Provost et al., 2018; Le Roy et al., 2019) have shown that the amplitude, A, of the seismic signal induced by a rockfall is related to its volume, V in a complex manner, that can be summarized as a power-law:

$$V = c.A^{\alpha} \tag{1}$$

https://doi.org/10.5194/egusphere-2026-3939
Preprint. Discussion started: 12 August 2026

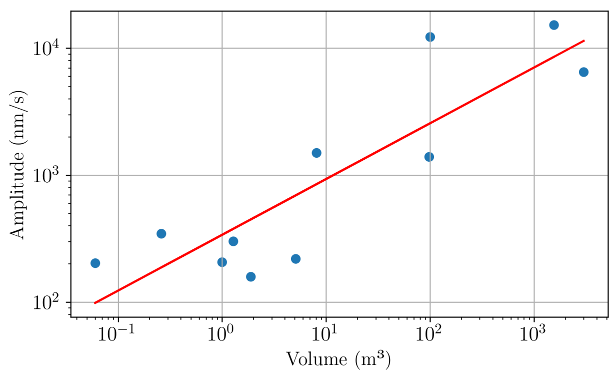

Figure 2. Log-log relationship between seismic amplitude and rockfall volume.

In the seismic catalog, the volume of 11 recorded rockfalls has been estimated using diachronic relief measurements (Le Roy et al., 2019). This small amount prevents us to include volume estimates in our analysis, but allows to verify the relationship between the seismic signal amplitude and the rockfall volume. As a result, our data are consistent with equation 1.

Figure 2 shows the empirical relationship between amplitude and volume and the fitted relationship yields a scaling exponent $\alpha = 0.44$ and a coefficient $c = 338$, indicating that rockfall volume increases proportionally with amplitude according to $V = 338.A^{0.44}$. Despite the limited number of rockfall events with volume, this result confirms the use of amplitude as an indicator of the relative size of rockfalls throughout the catalog.

Figure 3 shows the cumulative distribution of rockfall event seismic amplitude. This distribution appears to be well described by a power-law.

$$P(\geq A) = c.A^{-b} \tag{2}$$

where $P(\geq A)$ represents the cumulative distribution of rockfall events with seismic amplitude greater than A, a is the normalisation constant, and b the decay exponent. Considering the power-law relationship of equation 1, the empirical distribution of volume also follows a power-law, as usually observed for rockfall catalogs (Dussauge et al., 2003; Graber and Santi, 2022). This linear relationship on a logarithmic scale implies that large rockfalls are much less frequent than small ones.

We used the method provided by Clauset et al. (2009), based on maximum likelihood, for determining the lower cut-off of 520 nm/s, caused by the incomplete detection of smallest events, and the exponent of 1.18.

For the period 2013-2024, 657 rockfalls have been detected, corresponding to an average of approximately five rockfalls per month. We analyze the rockfall data along two axes: time and amplitude. First, we examine the occurrence of events by month over a ten-year period as well as the monthly average amplitude of the events to identify seasonal trends. Then, we study the amplitude distribution to highlight the relationship between the frequency and amplitude of rockfall events.

[0]Observatoire des Mouvements et Instabilités de Versant (OMIV)

https://doi.org/10.5194/egusphere-2026-3939
Preprint. Discussion started: 12 August 2026

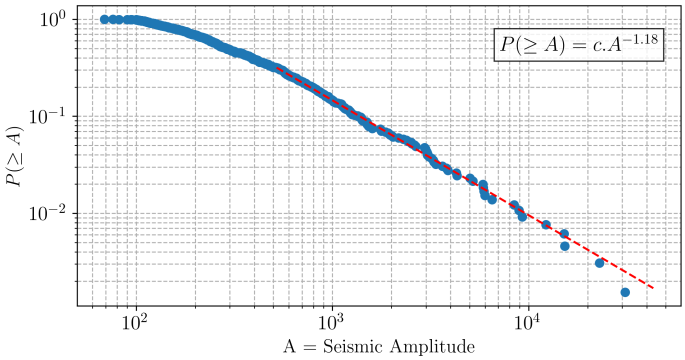

Figure 3. Complementary cumulative distribution function of rockfall amplitudes.

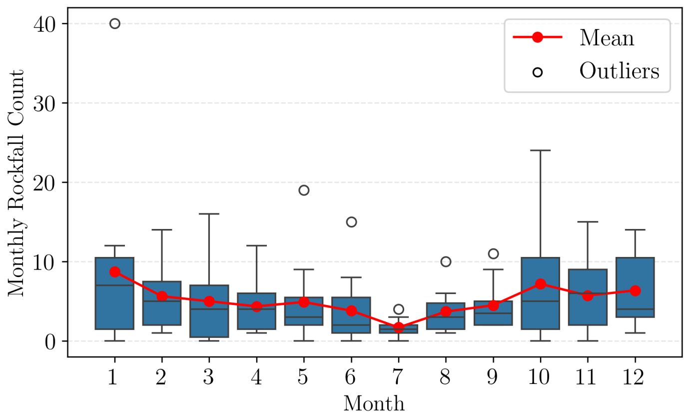

Figure 4. Box-plot of rockfall events per month over 10 years.

Figure 4 shows the mean and median number of rockfalls per month over a ten-year period. One may observe that the rockfall activity is dependent on the month. The highest activity is observed in January, with a mean value of approximately 8.5 rockfall per month. October, November, and December also show relatively high values exceeding 6 rockfalls on average, while July exhibits the lowest activity, with fewer than 2 rockfalls per month. This suggests a seasonal trend in rockfall occurrence with a **higher** frequency of rockfall events in winter (particularly in January) and autumn (October and November), while the **lowest** frequency is observed in summer (especially in July). Monthly activity shows considerable variability over the ten-year period analyzed. The median values are generally lower than the mean, suggesting that most months show a moderate rockfall activity with a limited number of months that notably increase the average number of events. The presence of outliers in the monthly distributions indicates that there are individual month-year combinations characterized by high rockfall activity.

https://doi.org/10.5194/egusphere-2026-3939
Preprint. Discussion started: 12 August 2026

2.1.2 Precipitation Time Series

In order to analyze the potential relationship between rain and rockfall, we used data provided by Météo-France for the Grenoble-LVD station located within 5 km radius of the Saint Eynard site (data available at Météo-France Open Data portal). This high-resolution dataset provides cumulative precipitation, h, over the time step of one hour over the full period of ten years of the rockfall catalog. In order to consider larger time scales, wecomputed daily and monthly cumulative rainfall. We aim to extract insights from two perspectives: the temporal one and the intensity one. The first focuses on the daily scale, which is the most granular and precise, followed by a monthly description to identify seasonal trends and an analysis of consecutive rainy days. Finally, the second perspective focuses on intensity by analyzing the daily distribution of precipitation to identify rainfall regimes.

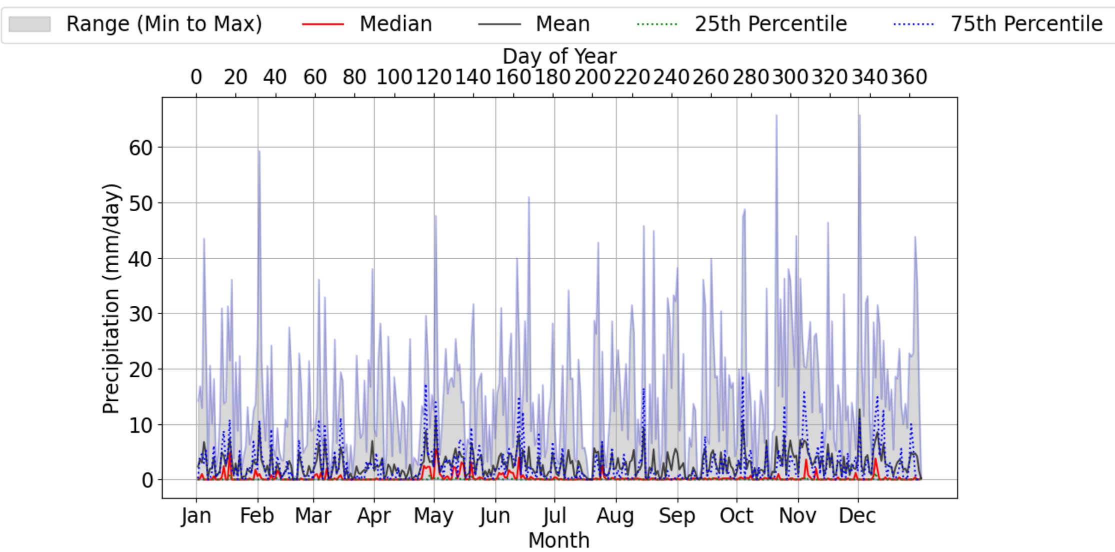

Figure 5. Statistics of daily precipitation for each day of the year (2013-2024).

Figure 5 shows that the median precipitation is generally very low throughout the year. The maximum daily precipitation varies significantly from day to day, with notable peaks observed at different times of the year (two high peaks in February and October, reaching or exceeding 60 mm/day). Percentiles illustrate the distribution of precipitation: the 25$^{\text{th}}$ percentile remains very low, while the 75$^{\text{th}}$ percentile increases markedly, particularly during periods of heavy rainfall.

Figure 6 presents monthly precipitation trends over a ten-year period. It shows that precipitation variability is higher in winter and late spring compared to the summer period. Additionally, the red line representing the average precipitation for each month follows a similar trend. Overall, rainfall can be observed throughout the year.

Figure 7 shows the histogram of consecutive rainy-day sequences, where a rainy day is defined as a day with non-zero precipitation. First, we found that the maximum length of a rainy sequence is 14 days. Therefore, we use this duration as the maximum time scale of retrospective horizon RH). The distribution clearly indicates that short rainy sequences are much more

https://doi.org/10.5194/egusphere-2026-3939
Preprint. Discussion started: 12 August 2026

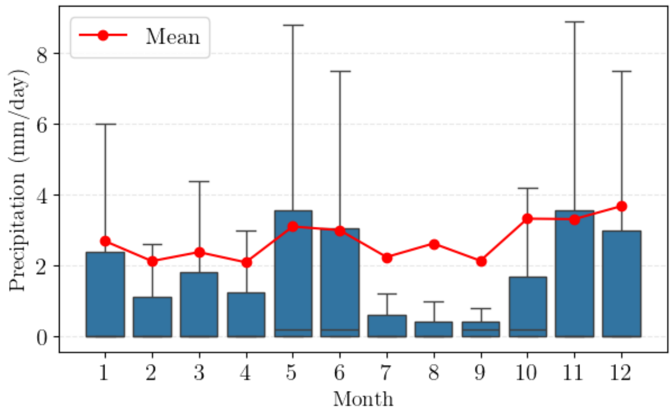

Figure 6. Box-plot of rainfall per month over 10 years.

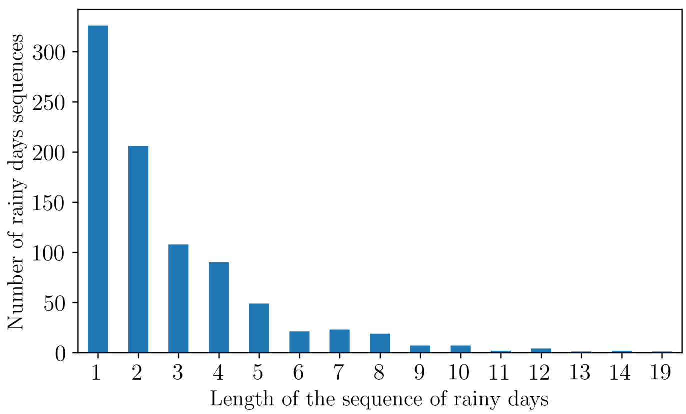

Figure 7. Occurrence of consecutive rain sequences.

frequent than long ones. Most precipitation episodes last one to two days, with a sharply decreasing frequency for sequences longer than five days.

https://doi.org/10.5194/egusphere-2026-3939
Preprint. Discussion started: 12 August 2026

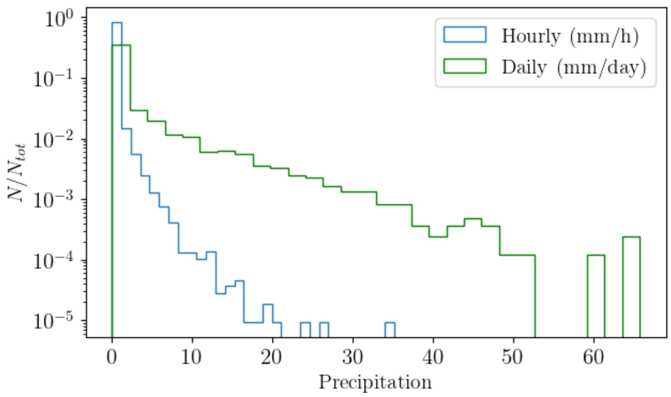

Figure 8. Distribution of rainfall.

The distribution of the daily cumulative precipitation is illustrated in Figure 8, where N is the number of days within each precipitation bin and N_{tot} is the total number of observed days. We observe that low precipitation levels (0-10 mm/day) are the most common, with approximately 75% of days recording very low precipitation (less than 2 mm/day). Occurrences decrease exponentially with increasing precipitation, indicating that heavy rainfall (beyond 40 mm/day) is less frequent. Note that a few extreme rainy days reach more than 60 mm/day.

2.1.3 Temperature Time Series

The temperature time series dataset was recorded at an hourly resolution over a ten-year period.

Figure 9 illustrates the seasonal trend of daily temperatures over the period 2013–2024. It can be observed that from January to February, most average temperatures are below 0°C. The median and mean temperatures gradually increase over the following months. June through August represent the warmest period of the year, with median and mean temperatures ranging between 20°C and 25°C. In September and October, temperatures gradually decrease and continue to drop through November and December, reaching values close to or below 0°C.

Next, we explore the potential correlations between precipitation, freezing and rockfalls, particularly by identifying the periods of rockfall associated with episodes of precipitation. To this end, we will begin the following section by defining the probabilities involved.

2.2 Distributions of meteorological factors and their association with rockfalls events

Understanding how meteorological conditions during rockfall events differ from those observed overall is the key to identifying potential triggers. Such comparisons reveal whether specific levels or patterns of a given factor are more likely to be associated with rockfall activity.

To explore this, we compare the distribution of relevant meteorological factors such as rainfall and temperature, at both the hourly and daily scales. The distributions are expressed in terms of relative frequencies, defined as the ratio between the

https://doi.org/10.5194/egusphere-2026-3939
Preprint. Discussion started: 12 August 2026

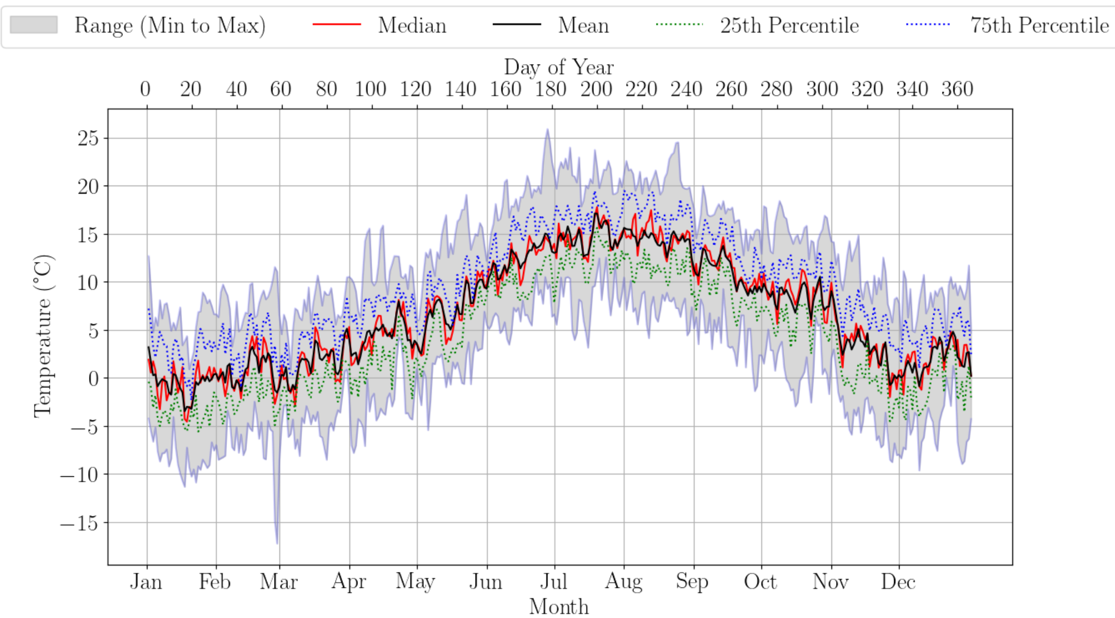

Figure 9. Temperature statistics for each day of the year (2013–2024).

number of occurrences within a given meteorological class and the total number of observations. These relative frequencies correspond to empirical probabilities, and are therefore denoted P(.) in the following.

$$\mathcal{P}(\mathrm{M}) = \frac{N(M)}{N_{tot}} \tag{3}$$

where M is the meteorological factor (rain/temperature), N(M) is the number of observations within class M and N_{tot} is the total number of meteorological observations.

We also compute the probability of a meteorological factor conditional on the occurrence of a rockfall defined as $\mathcal{P}(M \mid RF)$, where RF represents the occurrence of a rockfall event. Then, we quantify this relationship using the lift metric, defined as the ratio between the conditional probability of a meteorological factor M given a rockfall event and its marginal probability.

$$LIFT(M) = \frac{\mathcal{P}(M|RF)}{\mathcal{P}(M)} \tag{4}$$

This ratio indicates how much more or less a given level of the factor can be associated with a rockfall compared to its general occurrence.

The following analysis is applied to the rainfall and temperature meteorological variables. For each case, distributions are expressed as frequencies, which are later referred to as empirical probabilities.

https://doi.org/10.5194/egusphere-2026-3939
Preprint. Discussion started: 12 August 2026

2.2.1 Rainfall distributions

The distribution of all observed rainfall events is represented in blue, those associated with rockfall events are represented in green and the ratio of the two distributions is represented in red (see figure 10).

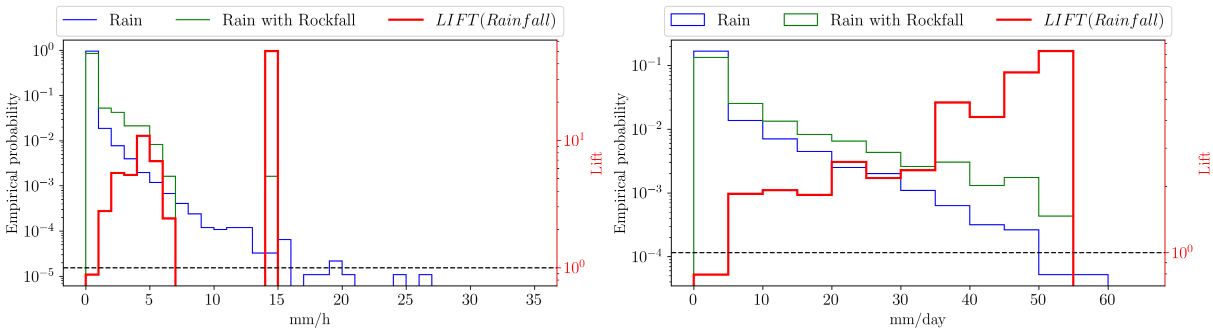

(a) Hourly distribution.

(b) Daily distribution.

Figure 10. Distribution of rainfall and its association with rockfall events.

At an hourly scale, the ratio between the rainfall distribution during rockfall events and the overall rainfall distribution indicates an over-representation in the 2–7 mm/h and 14-15 mm/h ranges, meaning rockfall events occur more frequently for these rainfall intensities than expected.

At a daily scale, rockfall events appear consistently over-represented across most rainfall intensities, with a clear amplification above 20 mm/day. This may indicate that the higher the rainfall intensity accumulated over a day, the stronger its influence on rockfall occurrence compared to hourly intensities.

2.2.2 Temperature distributions

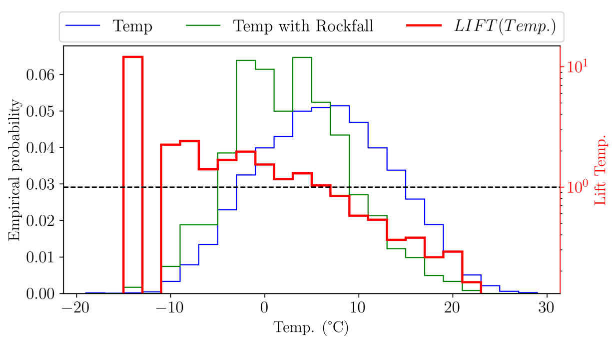

Figure 11. Distribution of hourly temperature and its association with rockfall events.

https://doi.org/10.5194/egusphere-2026-3939
Preprint. Discussion started: 12 August 2026

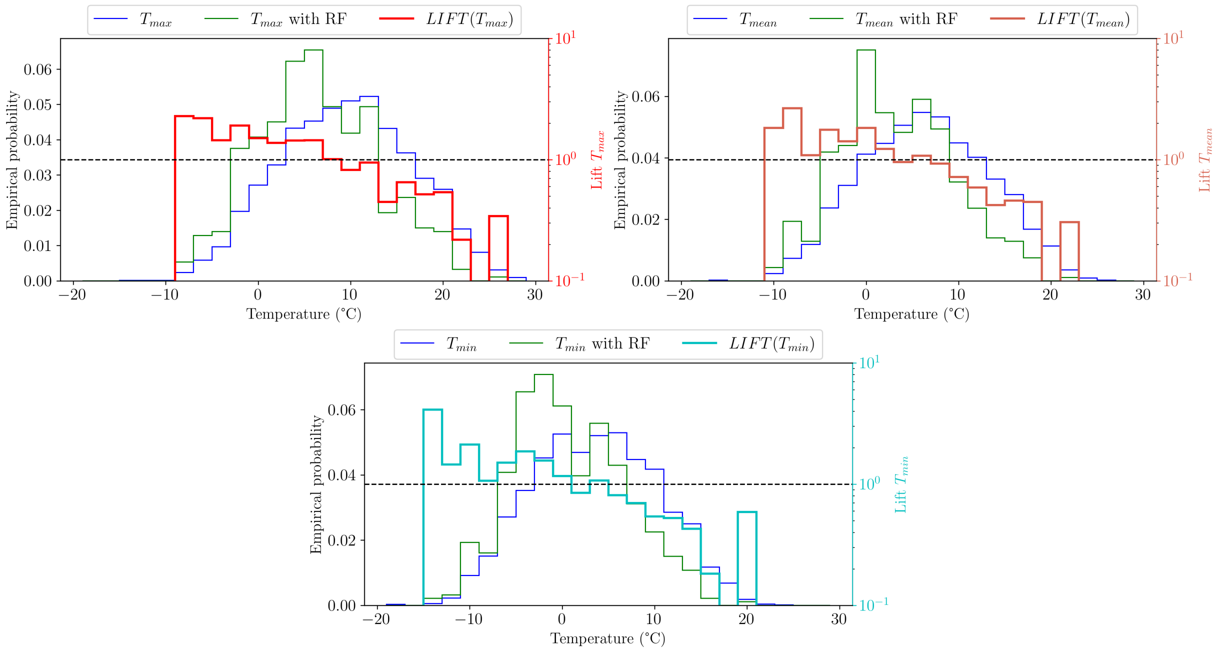

Figure 12. Distribution of daily minimum, mean and maximum temperature and their association with rockfall events.

Figure 11 illustrates that the overall temperature distribution in blue shows most occurrences between 0°C and 25°C. Also, the temperature distribution during rockfall events in green has a similar shape but is slightly more concentrated in specific ranges, particularly in lower temperatures. The red curve shows a high over-representation of rockfall occurrences at temperatures below 5°C, especially around -10°C to 5°C, indicating a strong freeze–thaw effect as a rockfall trigger.

Figure 12 presents the distributions of daily maximum, mean and minimum temperatures for all days and for days associated with rockfall events, with the corresponding lift values.

We notice that the distributions of temperature associated with rockfall are slightly shifted towards lower temperature compared to the general distribution. For maximum temperature it is over-represented at low to moderate temperature -9°C to 7°C and under-represented at high temperatures. A similar pattern is observed for the mean temperature. Similarly, this ratio is over-represented during days with minimum temperature from -15°C to 0°C. This may indicate that minimum temperature below 0°C and freezing plays a significant role in triggering rockfalls.

For this reason, the following analyses will focus on daily aggregation of precipitation and temperature, as it gives a more pronounced over-representation compared to the hourly resolution.

2.3 Cross-Correlation Analysis

In order to explore how environmental factors influence rockfall activity over time, we carried out a cross-correlation analysis for the rainfall–rockfall relationship using Bourke (1996) Cross-correlation (CC):

https://doi.org/10.5194/egusphere-2026-3939
Preprint. Discussion started: 12 August 2026

$$C_k(X,Y) = \frac{\sum(X_t - \overline{X})(Y_{t-k} - \overline{Y})}{\sqrt{\sum(X_t - \overline{X})^2 \sum(Y_{t-k} - \overline{Y})^2}} \tag{5}$$

where :

- X_t: binary value representing the rockfall occurrences at time t, with $X_t = 1$ if at least one rockfall event is observed and $X_t = 0$ otherwise.
- Y_t: value of the environmental variable (rainfall intensity or temperature) at time t.
- $\overline{X}$: mean of the time series X.
- $\overline{Y}$: mean of the time series Y.
- k: time lag, representing how far we shift one time series relatively to the other.

This analysis helps us to quantify the temporal relationship and identify any time lags at which rainfall are most strongly linked to rockfall events. By studying these relationships, we can figure out whether rockfalls happen right after a rainfall shift, or whether there is a delayed reaction.

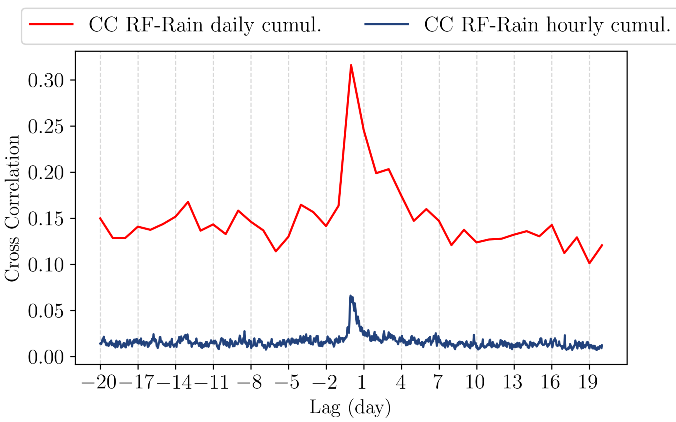

Figure 13. Cross-correlations between rockfall and rainfall considering the hourly and daily cumulated rain.

Figure 13 presents the (CC) between rainfall and rockfall occurrence depending on the temporal aggregation precipitation. When rainfall is considered at the hourly scale, the correlation with binary rockfall occurrence remains low with only a weak peak around lag 0. But, when rainfall is accumulated over one day, the correlation is significantly higher and shows a sharp maximum at lag 0 and maintains an elevated level for about 2–3 days. This temporal pattern is consistent with expert-based rules used in rockfall prediction.

These results indicate that rockfall occurrence is more strongly associated with daily aggregated rainfall than with hourly precipitation, highlighting the strong influence of recent rainfall on rockfall occurrence. It can be interpreted as the fact that the time scale of the physical phenomenon is larger than the hourly scale and is more relevant at a daily scale.

https://doi.org/10.5194/egusphere-2026-3939
Preprint. Discussion started: 12 August 2026

3 Empirical Conditional Probability analysis and results

3.1 Methodology

The initial dataset can be transformed into a new dataset, as a set of event occurrences, defined as:

$$\mathcal{D} = \{(d_1, e_1), (d_2, e_2), \ldots, (d_n, e_n)\}$$

where each pair (d_i, e_i) represents a day d_i and an event e_i, where i denotes the chronological order of days. The events e_i can be defined as:

$$e_i \in \{p\,, \overline{p}\,, r\,, \overline{r}\,, t_f\,, \overline{t_f}\,\}$$

with:

- p: precipitation > 0 mm.
- $\overline{p}$: precipitation $= 0$ mm.
- t_f: temperature < 0 °C.
- $\overline{t_f}$: temperature ≥ 0 °C.
- r: at least one rockfall occurred during the day.
- $\overline{r}$: no rockfall occurred during the day.

Observations

d_{-k_R}, e	$\cdots$	d_{-1}, e	d_1, e	d_2, e	$\cdots$	d_{k_P}, e

$\underbrace{\qquad\qquad M/\overline{M} \qquad\qquad}$ $\underbrace{\qquad\qquad R/\overline{R} \qquad\qquad}$

Retrospective Horizon (RH) Forecast Horizon (FH)

Our dataset becomes $\mathcal{O}$, the set of observations. An observation is defined as the action of analyzing phenomena within a time series $\mathcal{D}$. Each observation is defined with respect to a specific observation point d_1 in the temporal space, which separates the past and the future temporal information. From this observation point, two temporal horizons are considered: a retrospective horizon and a forecast horizon. These are denoted RH and FH, respectively and each observation is represented as a pair of temporal horizons (RH, FH).

– RH: An ordered list of consecutive days in $\mathcal{D}$. It is defined as a period of k_R consecutive days preceding the observation day d_1, constructed from D and expressed as:

$$RH = \langle d_{-k_R}, d_{-k_R-1}, \ldots, d_{-1} \rangle$$

https://doi.org/10.5194/egusphere-2026-3939
Preprint. Discussion started: 12 August 2026

RH allows us to observe a random variable M representing a meteorological factor under study (precipitation or freezing temperature) during the retrospective period:

- $M = 1$: the meteorological condition of interest (continuous precipitation or freezing temperatures) is present throughout the RH period.

$$M = 1 \iff \forall j \in \{-k_R, \dots, -1\}, \exists (d_j, e_j) \in \mathcal{D} \mid e_j = m$$

with $m \in \{p\,,t_f\}$

- $M = 0$: At least one day in RH period does not meet the condition (at least one dry day or a day above freezing)

$$M = 0 \iff \exists j \in \{-k_R, \dots, -1\}, (d_j, E_j) \in \mathcal{D} \mid e_j = \overline{m}$$

with $\overline{m} \in \{\overline{p}\,,\overline{t_f}\}$

– FH: An ordered subset of consecutive days in $\mathcal{D}$. It is defined as a period of k_P consecutive days starting from d_1, constructed from D and expressed as:

$$FH = \langle d_1, d_2, \dots, d_{k_P} \rangle$$

where we observe whether a rockfall (r) occurred or not ($\overline{r}$).

FH allows us to observe a variable R such that:

- $R = 1$: At least one rockfall occurred during the FH period.

$$R = 1 \iff \exists j \in \{1, \dots, k_P\}, (d_j, E_j) \in \mathcal{D} \mid e_j = r$$

- $R = 0$: No rockfall occurred during the FH period.

$$R = 0 \iff \forall j \in \{1, \dots, k_P\}, \exists (d_j, e_j) \in \mathcal{D} \mid e_j = \overline{r}$$

All probabilities used in this study correspond to empirical probabilities, estimated from the relative frequency of events within the dataset $\mathcal{O}$. For the sake of clarity, we simply refer to these empirical estimates as "probability $\mathcal{P}$" throughout the paper.

Several conditional probabilities are analyzed to assess the relationship between rainfall/temperature and rockfall events.

$$\mathcal{P}(R = 1 \mid M = 1) = \frac{\mathcal{P}(R = 1 \cap M = 1)}{\mathcal{P}(M = 1)} \tag{6}$$

The specific condition M used will be detailed in the corresponding sections.

We acknowledge that probabilities alone are not always sufficient to provide a reliable assessment of rockfall occurrence. To enhance confidence in our probability estimates, we introduce additional metrics that consider the population size, statistical dependencies, and baseline probability comparisons.

https://doi.org/10.5194/egusphere-2026-3939
Preprint. Discussion started: 12 August 2026

- To ensure that the derived probabilities are based on a statistically significant number of events, we use the **Confidence Interval (CI)** which provides a range in which the true probability can be expected to lie. So, we use the asymptotic confidence interval Olivier (2024) based on the Wald method expressed by :

$$IC(p) = \left[f_n - u\sqrt{\frac{f_n(1-f_n)}{n}}, \quad f_n + u\sqrt{\frac{f_n(1-f_n)}{n}} \right] \tag{7}$$

  Where f_n is the sample proportion, n is the sample size and u represents the quantile of the standard normal distribution corresponding to the chosen confidence level.

- We conducted the **Chi-squared** independence test to see if rockfall events are significantly associated with meteorological conditions. The test statistic is computed as follows Coron (2020) :

$$\chi^2 = \sum_{m\in\{M,\overline{M}\}} \sum_{r\in\{R,\overline{R}\}} \frac{\left(O_{m,r} - E_{m,r}\right)^2}{E_{m,r}} \tag{8}$$

  where $O_{m,r}$ represents the observed number of days under the corresponding meteorological condition m and the state of rockfall r, and $E_{m,r}$ denotes the expected frequency for the meteorological condition m and the rockfall state r, assuming independence between the two variables.

$$E_{m,r} = \frac{(n_m * n_r)}{n}$$

  -n_r is the total number of observations at the rockfall state r.

  -n_m is the total number of observations at the meteorological condition m.

  -n is the total sample size.

- To determine whether the rockfall probability under a specific condition differs significantly from the baseline rockfall probability, computed over the entire dataset, we estimate the **lift** metric, previously introduced in Equation(4).

  A lift value greater than 1 indicates that the condition increases the probability of rockfall, whereas a value below 1 suggests a lower likelihood compared to the baseline El Mazouri et al. (2019); Tseng and Lin (2007).

Then, to obtain a complete evaluation, we define an aggregated score, S_i, which counts the number of metrics that indicate a significant relationship at a specific time step i. Mainly, we evaluate the strength and significance of the meteorological condition–rockfall relationship by combining the lift metric and p-value(χ^2).

Aggregation is computed at each time step i using the following formula:

$$S_i = \sum_{j=1}^{2} \mathbb{1}(M_j(i)) \tag{9}$$

where:

https://doi.org/10.5194/egusphere-2026-3939
Preprint. Discussion started: 12 August 2026

- $\mathbb{1}()$ is the indicator function, that equals 1 if the metric meets the significance criteria and 0 if not.

- $M_1(i) = \begin{cases} 1, & \text{if Lift}_i > 1, \\ 0, & \text{otherwise.} \end{cases}$

  The threshold of 1 for the lift indicates a positive correlation between the meteorological condition and rockfall.

- $M_2(i) = \begin{cases} 1, & \text{if p-value}_i(\chi^2) < 0.05, \\ 0, & \text{otherwise,} \end{cases}$

  The threshold of 0.05, which represents the significance level, indicates that below this value, the relationship between the two variables is statistically significant Craparo (2007).

The aggregated score $S_i \in \{0,1,2\}$ represents the level of agreement between the two metrics in identifying a significant time step. Despite providing information on uncertainty, incorporating the confidence interval of the conditional probability into the binary aggregation would mask uncertainty trends. Instead, it will be analyzed separately and used as a complementary source of information to support the interpretation of the aggregated metrics.

3.2 Probability of Rockfall Conditioned on rainfall

In this section, we analyze conditional probabilities to better understand the relationship between rainfall and rockfall occurrence. The analysis consists of evaluating:

A. An expert-based approach, where we test whether continuous rainfall over multiple days (RH) influences rockfall probability.

B. A physics-informed approach, in which we incorporate a physical law into the rainfall analysis to account for the dynamics of rainfall charge, considering how rainfall accumulates and dissipates over time.

3.2.1 Approach A: Continuous Rainfall with 2 scenarios

In this approach, we consider two scenarios: First, we consider continuous rainfall events without any intensity filtering. Second, we account for the variability in rainfall intensity over the RH period and in the rockfall amplitude, to capture the effect of rainfall intensity on the rockfall magnitude. Therefore, we apply our methodology defined in section 3.1 for both cases.

Unfiltered continuous rainfall analysis:

We directly compute the conditional probability of rockfall given continuous rainfall (here $M = P$) over the Retrospective horizon (RH). In this case, the meteorological condition of interest is continuous rainfall:

- $P = 1$, if continuous rainfall (> 0 mm on each day) occurs throughout the RH period, and $P = 0$, otherwise.

https://doi.org/10.5194/egusphere-2026-3939
Preprint. Discussion started: 12 August 2026

First, we set the size of RH and FH to 14 days, based on Figure 7, which shows that 14 days is the maximum length of continuous daily rainfall sequences, and Figure 13, which indicates that the maximum time lag observed is 14 days. Our objective is to determine the optimal horizon size that best captures the relationship between continuous rainfall and rockfall occurrence.

By replacing M with P in Equation (6), we obtain the following probability expression:

$$\mathcal{P}(R=1 \mid P=1) = \frac{\mathcal{P}(R=1 \cap P=1)}{\mathcal{P}(P=1)} \tag{10}$$

where:

- $\mathcal{P}(R=1 \cap P=1)$ is the probability that it rained ($P=1$) during the entire RH period preceding d_1 and that at least one rockfall ($R=1$) occurred during the FH period starting at d_1:

$$\mathcal{P}(R=1 \cap P=1) = \frac{N(R=1 \cap P=1)}{N_{\text{RH,FH}}} \tag{11}$$

  where:

  - $N(R=1 \cap P=1)$ is the number of observations where $R=1$ and $P=1$:

  $$N(R=1 \cap P=1) = |\{o \in \mathcal{O} \mid R=1 \cap P=1\}|$$

    with o as an observation and $\mathcal{O}$ as the set of observations.

  - $N_{\text{RH,FH}} = |\mathcal{O}|$ is the total number of observations, i.e. the number of (RH,FH) pairs.

- $\mathcal{P}(P=1)$ is the probability that it rained during the entire RH period:

$$\mathcal{P}(P=1) = \frac{N(P=1)}{N_{\text{RH,FH}}} \tag{12}$$

  - $N(P=1)$ is the number of observations where $P=1$.

Since the denominators (number of (RH,FH) observations) are identical, they cancel out as follows:

$$\mathcal{P}(R=1 \mid P=1) = \frac{N(R=1 \cap P=1)}{N(P=1)} \tag{13}$$

The number of rockfalls that occur after different lengths of continuous rain events (RH) is presented in Figure 14.

https://doi.org/10.5194/egusphere-2026-3939
Preprint. Discussion started: 12 August 2026

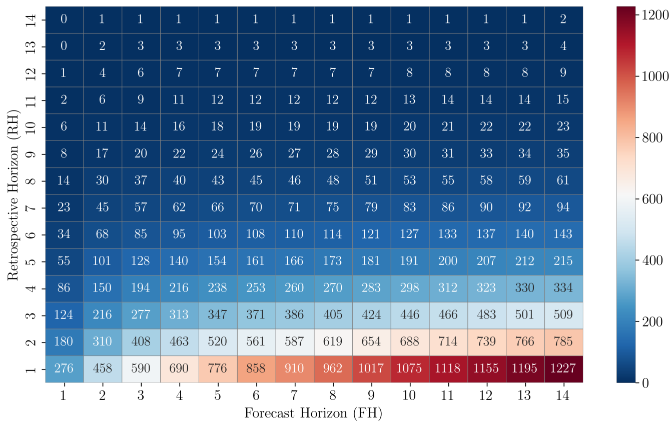

Figure 14. Heatmap of $|\{o \in \mathcal{O} \mid P = 1 \cap R = 1\}|$

As the retrospective horizon increases, the number of observations decreases. This is due to the fact that the number of rain episodes decreases as the size of the episodes increases. The highest numbers of observations are mainly located in the lower-right corner. This result indicates that rockfall events are more frequent when the FH is long after short periods of rain on RH. Furthermore,, a rockfall will always occur on high values of FH.

Now we examine the corresponding conditional probability in Figure 15.

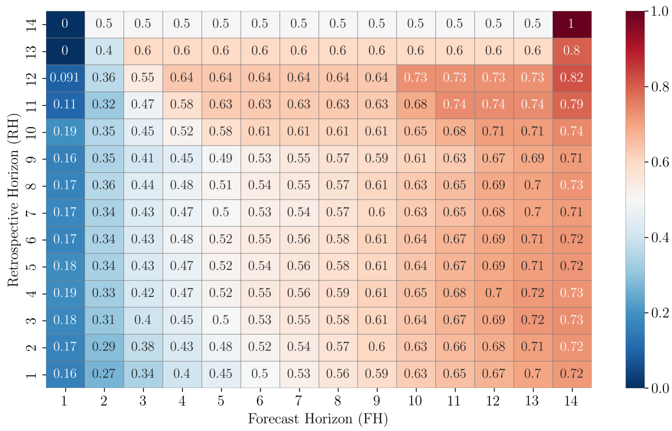

Figure 15. Heatmap of $\mathcal{P}(R = 1 \mid P = 1)$ as a function of RH and FH.

The conditional probability generally increases with both the retrospective horizon RH and the forecast horizon FH.The increase with FH is expected because longer forecast windows provide more opportunities for at least one rockfall to occur. Consequently, for long forecast horizons up to 14 days, the probability increases significantly with high values of RH to reach its maximum probability of 1. However, looking at Figure 14 we see that the number of observations is low in this combination

https://doi.org/10.5194/egusphere-2026-3939
Preprint. Discussion started: 12 August 2026

zone. Consequently, these high probabilities should be interpreted with caution, as they are not associated with a robust increase in rockfall occurrence. And for that reason, we compute the previously defined metrics: confidence interval, lift and p-value.

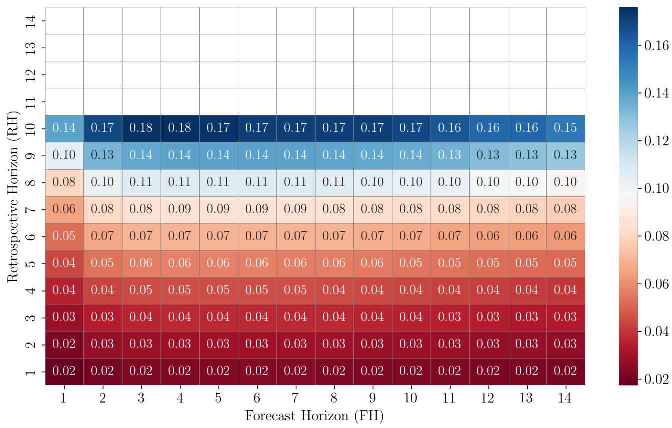

Figure 16. Results of Confidence Interval of $\mathcal{P}(R = 1 \mid P = 1)$.

Figure 16 shows the heatmap of confidence interval widths over different values of RH and FH and the color scale represents the width of the confidence interval. Small RH horizons are characterized by values (around 0.02) in the lower region, which indicates a more precise estimate when the confidence interval is narrow. The empty zone does not indicate an absence of rockfalls or confidence interval, but rather a lack of sufficient data to compute a reliable confidence interval, since the estimation of a confidence interval becomes statistically unstable for small sample sizes.

We used the χ^2 test to identify the dependence between rainfall and rockfall. Our null hypothesis H_0 states that rainfall and rockfall are independent. We set a significance level of $\alpha = 0.05$, which corresponds to the probability of incorrectly rejecting the null hypothesis.

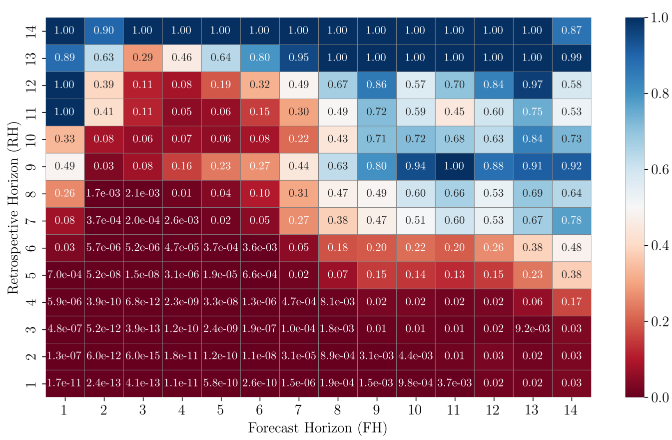

Figure 17. Results of the p-value from the χ^2 test.

https://doi.org/10.5194/egusphere-2026-3939
Preprint. Discussion started: 12 August 2026

A p-value lower than 0.05 indicates that we can reject the null hypothesis of independence, meaning there is a statistically significant relationship between the two variables, as shown in Figure 18. This allows us to identify specific periods where rainfall and rockfall are either independent or significantly related.

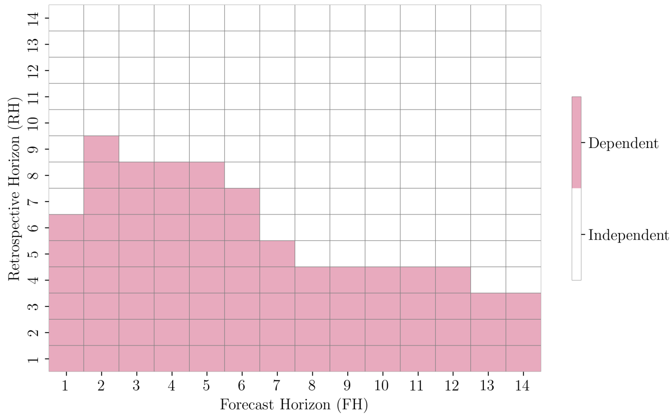

Figure 18. Results of the χ^2 independence test.

We observe that the two variables, rainfall and rockfall, are dependent for FH and RH values below 6 or 7 days. However, for the same RH horizon below 9 days, increasing FH makes the relationship with RH progressively more independent. This means that the dependence of rockfall on the RH condition is fading over time. Moreover, we observe that dependence is stronger for the second day and the third day on FH compared to the first day.

Then we compute the LIFT metric and in this case it is defined as follows:

$$LIFT = \frac{\mathcal{P}(R=1 \mid P=1)}{\mathcal{P}(R=1)} \tag{14}$$

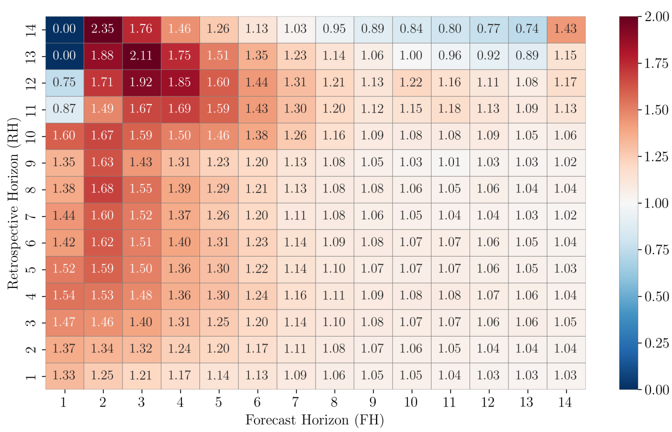

Figure 19. Heatmap of results of LIFT as a function of RH and FH.

https://doi.org/10.5194/egusphere-2026-3939
Preprint. Discussion started: 12 August 2026

Figure 19 shows that lift values are predominantly greater than 1 with a significant increase for high RH horizons (> 12) and short FH horizons (FH between 2 and 4 days), indicating that prolonged continuous rainfall conditioning increases the probability of rockfall occurrence. However, for shorter RH and longer FH horizons, lift values are close to 1, showing a weaker influence of rainfall continuity on delayed rockfall occurrence. Lift results indicate that continuous rainfall acts more as a short-term trigger rather than a long-term conditioning factor.

As described in the first Section 3.1 in our methodology, a binary value was assigned to the lift and the χ^2 test p-value metrics based on their significance: a score of 1 indicates that the metric is significant, while a score of 0 means it is not. Each $RH - FH$ combination is classified based on whether it simultaneously satisfies these two criteria, by using equation 9, which leads to the aggregated significance map shown in Figure 20.

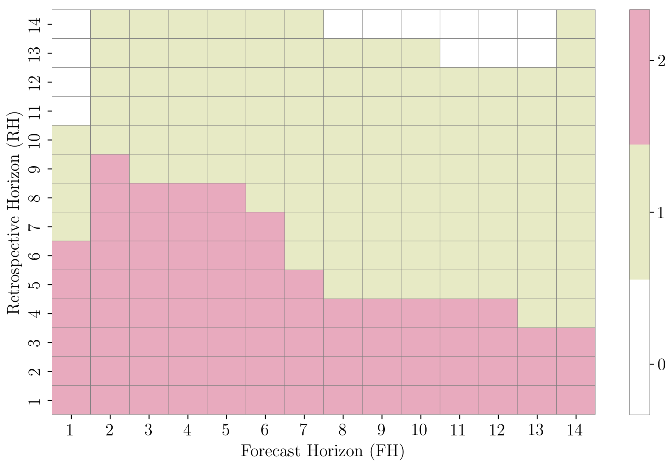

Figure 20. Results of metrics aggregation over the RH and FH horizons.

This aggregation shows a region of statistically significant with the strongest relationship between rainfall and rockfall occurrence for retrospective periods RH = 1 to 9 days, across a wide range of FH (1–14 days). As RH increases, the dependence weakens, meaning past rainfall beyond 9 days has less impact on predicting rockfalls.

The confidence interval (CI), presented in Figure 16 can be used as a complementary indicator to our final aggregation. By examining this CI heatmap under different thresholds, a progressive reduction of the significant period is observed by consulting a lower margin of error. For example, if we impose a stricter CI constraint (CI width $< 5\%$) it significantly reduces the range of RH. While the aggregated measures significance is up to RH = 9 days, the additional information provided by CI shows that low uncertainty estimates refine the period to an RH = 1 to 5 days.

https://doi.org/10.5194/egusphere-2026-3939
Preprint. Discussion started: 12 August 2026

Threshold-Based Analysis:

While the previous analysis considered the overall temporal relationship between rainfall and rockfall, it did not account for the variability in rainfall intensity and rockfall amplitude. To better capture these dynamics, we introduce a threshold-based approach, where rainfall intensity and rockfall amplitude are categorized into two levels (low and high).

For threshold selection, we used a quantile-based approach.

- Rainfall intensity: we set the threshold $\mathrm{Thr}_{\mathrm{int}}$ at the 95^{th} percentile which corresponds to the top 5% of the heaviest rainfall events. Based on Figure 8, this threshold $\mathrm{Thr}_{\mathrm{int}}$ is 16.42 mm of precipitation. This ensures that any daily precipitation above this value is classified as intense rainfall, while values below this threshold are classified as low-intensity rainfall.

- Rockfall amplitude: we selected the 90^{th} percentile of rockfall amplitudes. The computed threshold $\mathrm{Thr}_{\mathrm{amp}}$ is 1347.30 nm/s. So, if the amplitude exceeds this value, it is classified as a high amplitude rockfall else it is considered as lower-amplitude rockfall.

In the previous analysis the meteorological condition M was simply the presence of continuous rainfall. Here, we refine M to incorporate intensity thresholds distinguishing between high and low-intensity rainfall events.

Thus, we redefine M as follows:

- **Heavy Rainfall** ($M = P_{heavy} = 1$): continuous rainfall (> 0 mm on each day) over RH where at least one daily precipitation event has an intensity $\geq \mathrm{Thr}_{\mathrm{int}}$.

- **Low Rainfall** ($M = P_{heavy} = 0$): continuous rainfall over RH where all daily precipitation intensities remain $< \mathrm{Thr}_{\mathrm{int}}$.

Similarly, we classify rockfall events based on their amplitude:

- **Large Rockfall** ($R = 1$): at least one rockfall event occurs over the FH with an amplitude $\geq \mathrm{Thr}_{\mathrm{amp}}$.

- **Small Rockfall** ($R = 0$): no rockfall event over FH with an amplitude $\geq \mathrm{Thr}_{\mathrm{amp}}$.

Using these definitions, we compute the conditional probabilities of rockfall occurrence under four distinct cases:

- $\mathcal{P}(P_{heavy} = 1 | R_{Large} = 1)$ as Heavy Rainfall-Large Rockfall.

- $\mathcal{P}(P_{heavy} = 1 | R_{Large} = 0)$ as Heavy Rainfall-Small Rockfall.

- $\mathcal{P}(P_{heavy} = 0 | R_{Large} = 1)$ as Low Rainfall-Large Rockfall.

- $\mathcal{P}(P_{heavy} = 0 | R_{Large} = 0)$ as Low Rainfall-Small Rockfall.

This approach allows us to better understand the influence of different levels of rainfall events on rockfall probability and identify key periods where these relationships are most significant.

https://doi.org/10.5194/egusphere-2026-3939
Preprint. Discussion started: 12 August 2026

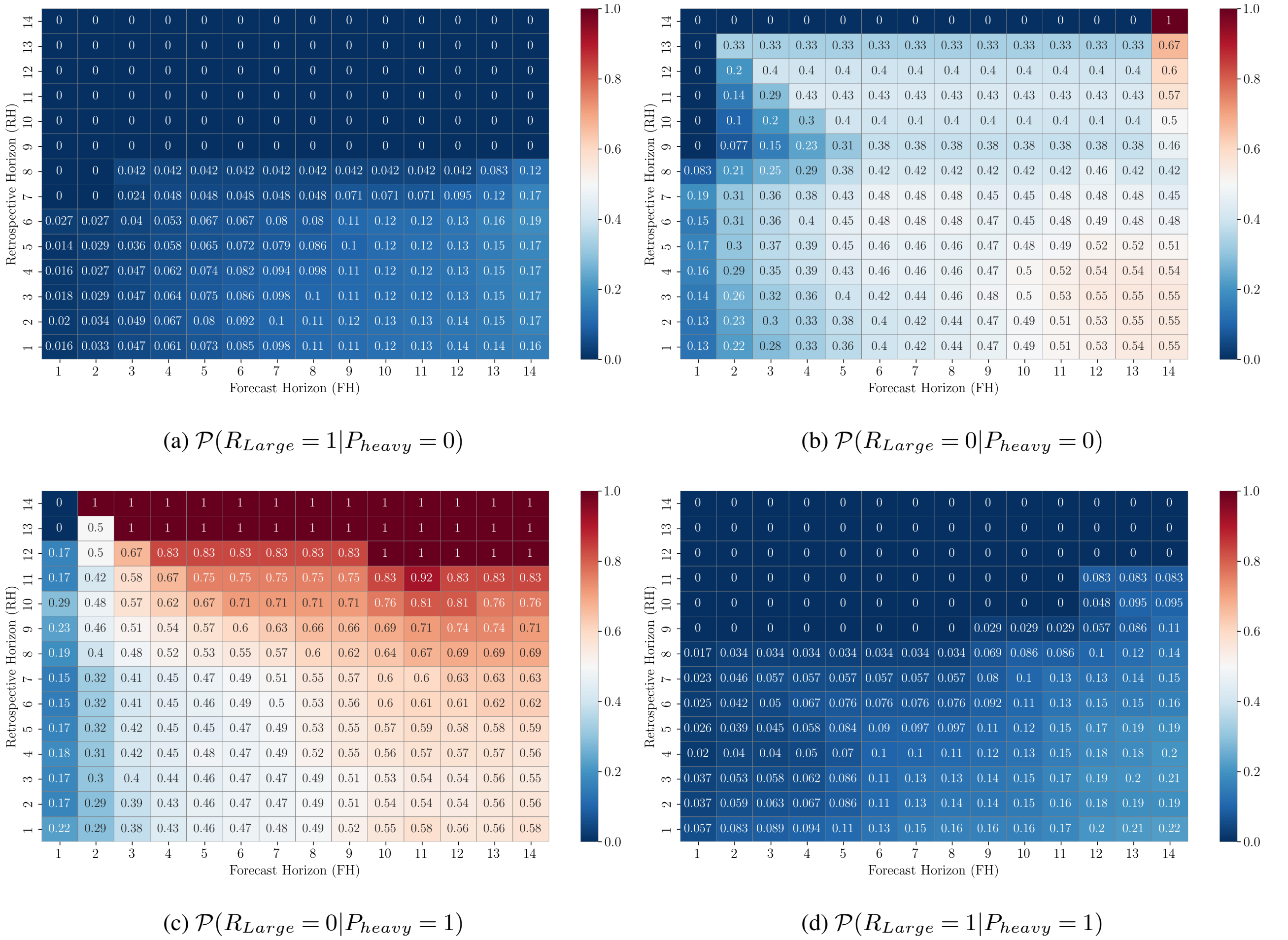

(a) $\mathcal{P}(R_{Large} = 1 | P_{heavy} = 0)$ (b) $\mathcal{P}(R_{Large} = 0 | P_{heavy} = 0)$

(c) $\mathcal{P}(R_{Large} = 0 | P_{heavy} = 1)$ (d) $\mathcal{P}(R_{Large} = 1 | P_{heavy} = 1)$

Figure 21. Results of probability of different cases as a function of RH and FH.

The resulting probability maps are shown in Figure 21, highlighting a marked contrasts. Indeed, the probability of large rockfall occurrence is generally higher under heavy rainfall conditions than under low rainfall, particularly for short retrospective horizons. On the other hand, small rockfall occurrence is higher under heavy rainfall than under low rainfall.

To identify the most significant temporal horizons, we apply our defined methodology based on the lift metric and the p-value of the χ^2 test. A binary score is assigned to each metric for each period (RH, FH) based on statistical significance (1 if significant, 0 otherwise). The final aggregated results highlight the key horizons where rainfall intensity significantly influences rockfall occurrence of different magnitudes. And, we then analyse the confidence interval at different uncertainty thresholds, which can help us refine the significant horizons.

The results highlight a contrasting influence of rainfall on rockfalls depending on their intensity and magnitude.

From Figure 22 (a) and (b), we can see the rockfalls triggered by low rainfall. For large rockfalls (a), the χ^2 tests are almost entirely absent, indicating that under low rainfall conditions, large rockfalls are not statistically associated with rainfall

https://doi.org/10.5194/egusphere-2026-3939
Preprint. Discussion started: 12 August 2026

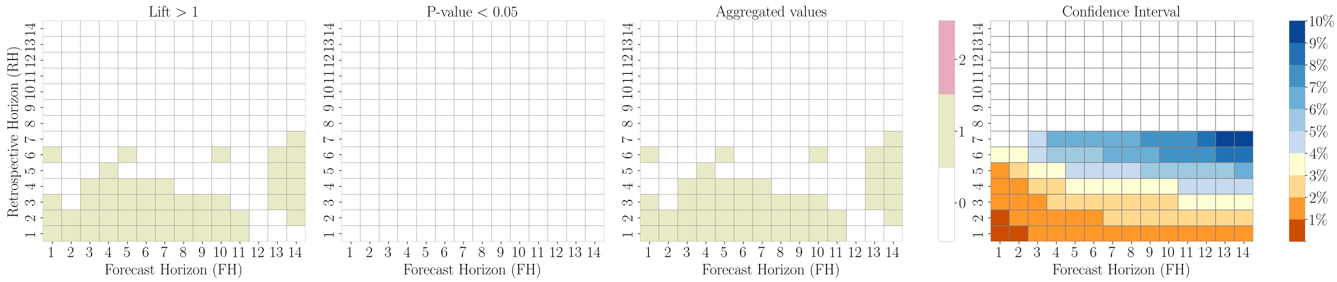

(a) $\mathcal{P}(R_{Large} = 1 | P_{heavy} = 0)$

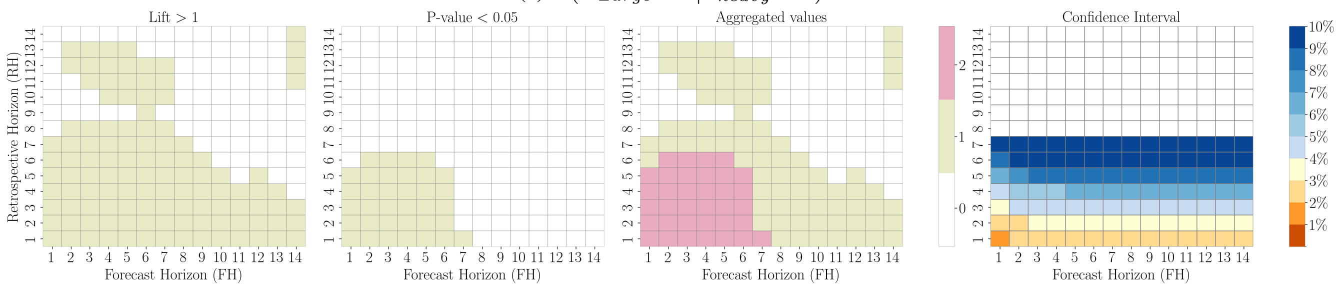

(b) $\mathcal{P}(R_{Large} = 0 | P_{heavy} = 0)$

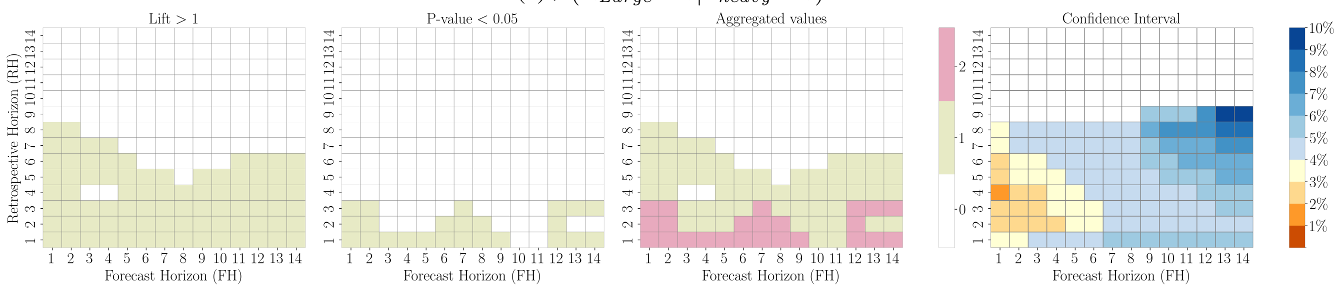

(c) $\mathcal{P}(R_{Large} = 1 | P_{heavy} = 1)$

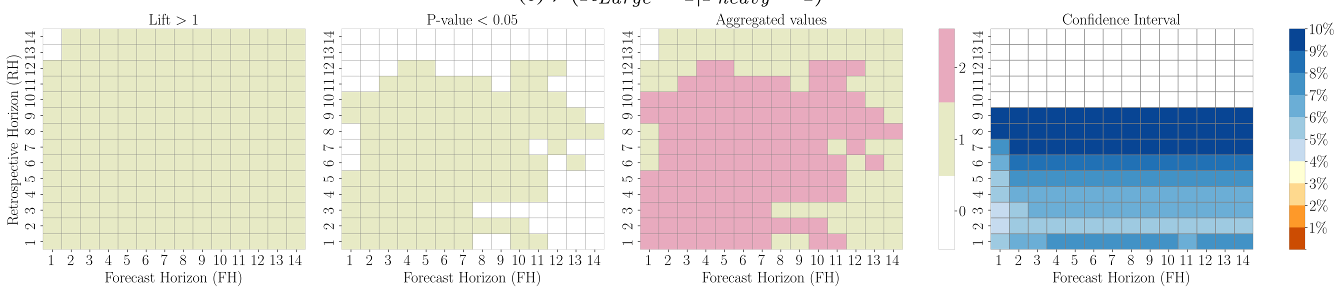

(d) $\mathcal{P}(R_{Large} = 0 | P_{heavy} = 1)$

Figure 22. A binary masking of Lift and p-value metrics and their aggregated score indicating the number of satisfying the two criteria, followed by a complementary information of CI across varying thresholds for different rainfall and rockfall scenarios : (a) Low Rainfall - Large Rockfall ($P = 0, R = 1$), (b) Low Rainfall - Small Rockfall ($P = 0, R = 0$), (c) Heavy Rainfall - Large Rockfall ($P = 1, R = 1$), (d) Heavy Rainfall - Small Rockfall ($P = 1, R = 0$). Lower CI values correspond to lower uncertainty and higher values indicate higher uncertainty.

https://doi.org/10.5194/egusphere-2026-3939
Preprint. Discussion started: 12 August 2026

accumulation no matter the considered temporal horizons. However, for small rockfalls (b), metrics show significant values, indicating that those events under low rainfall conditions show a statistically significant associations. The final aggregation shows a significant temporal horizon regions ranging from 1 to 6 days for RH and forecast horizon up to 7 days. By taking into account the CI, it further refines our interpretation. Indeed, when considering the horizons with a low uncertainty (e.g. CI below 5%), the range of significant horizons is reduced to a RH up to 4 days. This indicates that the most confident influence of low rainfall on small rockfall occurrence especially is strongest in the first 4 days preceding the event. So while extended horizons may indicate potential influence, decision-makers can rely more confidently on shorter horizons associated with lower uncertainty of CI.

For heavy-rainfall conditions. For the first case (c) large rockfalls, most significant regions are mainly concentrated in a retrospective window of 1 to 3 days, combined with forecast horizons extending up to 14 days. The CI further shows that low margin of error levels focus on retrospective horizons up to 3-4 days. This may reflect a rapid saturation effect of the ground and an almost immediate response in terms of rockfall occurrence.

And for small rockfalls (case (d)), the effect is more diffuse, with a high significance observed in a retrospective window of 1 to 12 days across all the FH. However, the analysis of CI especially those associated with low uncertainty indicates that the most significant horizons are located within the RH from 2 to 3 days with a forecast horizon of one day. This suggests that small rockfalls may occur with a one day delay after heavy rainfall events.

3.2.2 Approach B: Rainfall Charge-Discharge(H)

This section considers the water storage and discharge in the cliff using a water charge function, H, inspired from hydrological analysis of rock massifs (Helmstetter and Garambois, 2010; Vallet, 2014).

Rainfall is considered as the inflow that increases the water storage. Afterward the storage decreases due to an outflow that follows an exponential rate depending on the current value of H. Unlike the earlier analysis with a predefined RH horizon for rainfall history, this approach introduces a decay coefficient λ, which controls how long the effects of past rainfall persist in the rock mass.

In absence of rainfall, H is modeled by an exponential decay function (Vallet, 2014):

$$H(t+\Delta t) = H(t) \cdot e^{-\Delta t/\lambda} \tag{15}$$

where:

- $H(t)$ is the charge at time t
- λ is the decay coefficient, which determines how slowly the charge decays over time
- Δt is the elapsed time since t.

The charge is updated after each rainfall considering that rainfall is added to actual value of H and applying the decay function:

https://doi.org/10.5194/egusphere-2026-3939
Preprint. Discussion started: 12 August 2026

$$H(t+\Delta t) = [H(t^-) + \mathrm{h}(t)]e^{-\Delta t/\lambda} \tag{16}$$

where:

- $H(t^-)$ is the charge at time t, just before the rainfall event
- $h(t)$ is the rainfall occurring at time t
- Δt is the elapsed time since the last rainfall.

The H function is calculated at each time step of the data set dt, i.e. 1 hour. Hence $h(t)$ is considered as the cumulative rainfall in the time range $[t-dt;t]$;

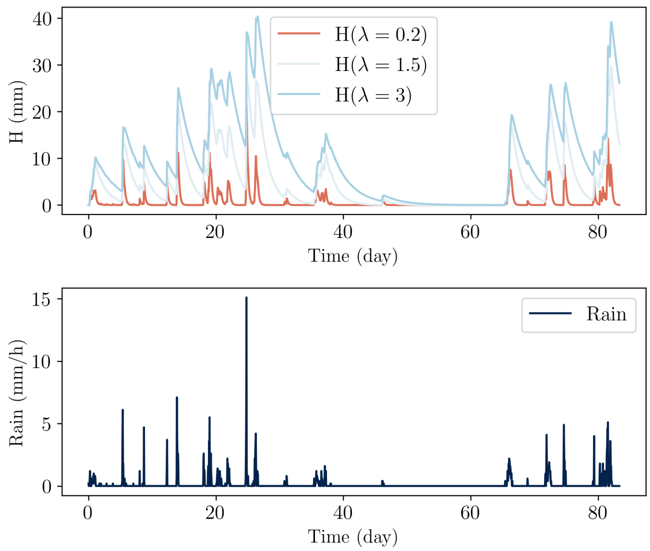

Figure 23. H fonction for different decay coefficient λ, over the period [15-10-2013, 06-01-2014].

Figure 23 illustrates how λ controls the temporal evolution of $H(t)$. A small value of λ leads to a rapid decrease in $H(t)$, so past rainfall dissipates quickly whereas a higher values of λ result in a slower decay, so rainfall events have an effect over a longer time period.

In this approach, the result of equation 16 is first computed at an hourly scale. And then, for the empirical conditional probability of rockfall given rainfall charge analysis we do not use the hourly values of H. Instead, we perform the study at the daily scale by extracting the maximum value of H for each day. This daily maximum represents the highest level of charge reached during the day. This daily indicator is then used in our defined methodology. We therefore need to find the optimal value of λ. Since the choice of λ is crucial, it influences how rainfall accumulation is represented.

Thus, we redefine M in this context as the meteorological condition related to the level of rainfall charge ($M = H_{level}$), meaning the conditional probability of rockfall is now computed:

https://doi.org/10.5194/egusphere-2026-3939
Preprint. Discussion started: 12 August 2026

$$\mathcal{P}(R=1 \mid H_{level}=1) = \frac{\mathcal{P}(R=1 \cap H_{level}=1)}{\mathcal{P}(H_{level}=1)} \tag{17}$$

We categorize H into four levels based on empirical thresholds. These thresholds are defined from the distribution of the daily maximum values of H, these maxima record the maximum charge reached on each day :

- $\mathbf{H_{low}}$: low charge (below the 5$^{\text{th}}$ percentile as shown on Figure 25 with the purple dashed line).
- $\mathbf{H_{medium}}$: medium charge, defined as values between the low and high thresholds.
- $\mathbf{H_{high}}$: high charge (threshold determined based on over-representation of high charges associated with rockfalls) as illustrated on Figure 25 with the red dashed line.
- $\mathbf{H_{global}}$ represents all events where $H > 0$, regardless of intensity. It will capture the overall influence of rainfall charge-discharge.

To determine the most informative value of λ, we compute the lift for each charge level H across different values of λ, using the following formula.

$$\text{LIFT}_{H_{\text{level}}} = \frac{P(\text{rockfall} \mid H_{\text{level}})}{P(\text{rockfall})} \tag{18}$$

As illustrated in Figure 24, the variation of lift with different values of λ highlights the impact of rainfall charge on rockfall probability.

The determined the most informative value of λ as the one fitting both criteria : λ:

- A λ that maximizes $\text{Lift}_{H_{\text{high}}}$, what indicates that a wet period (high charge) significantly increases the rockfall risk.
- A λ that minimizes $\text{Lift}_{H_{\text{low}}}$, what indicates that a dry period (low charge), reduces the rockfall risk.

So, after analyzing the obtained results, we selected $\lambda = 0.2$ as the optimal value.

Once λ is set, we examine the resulting distribution of the daily maximum values of H (see Figure 25).

With this selected λ, we can now analyze the conditional probability of rockfall occurrence given different charge levels ($H_{\text{global}}, H_{\text{low}}, H_{\text{medium}}, H_{\text{high}}$) and our metrics.

The results of probability of Figure 26 show a clear relation between the charge H (accumulated rainfall in the ground) and the likelihood of rockfall occurrence. When the charge is high, the probability of rockfall is slightly high even in the short periods FH and it keeps increasing over time. So when the ground is highly saturated, it does not take much more time to trigger a rockfall in the next days. Therefore, for low charge the initial probability is very low (about 0.07) but it progressively increases to reach 0.71 on day 14. So the greater the ground saturation, the higher the probability of rockfall. For medium intensity charge H_{medium} and H_{global} both they are following a similar trend, the probability starts lower and increases as FH increases. In general, the results indicate that increasing ground saturation systematically increases rockfall probability.

https://doi.org/10.5194/egusphere-2026-3939
Preprint. Discussion started: 12 August 2026

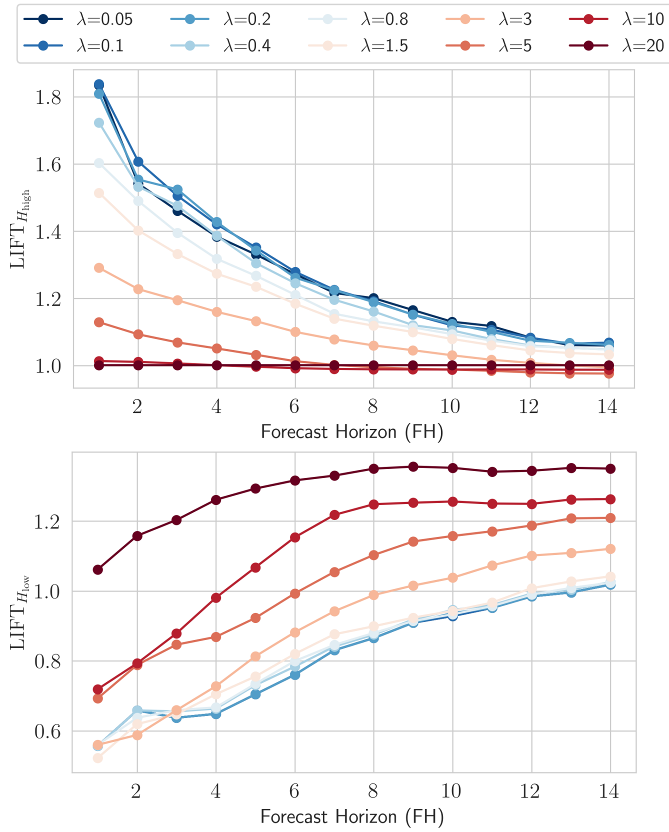

Figure 24. Lift values for different charge levels. The upper plot corresponds to H_{high}, while the bottom plot corresponds to H_{low}.

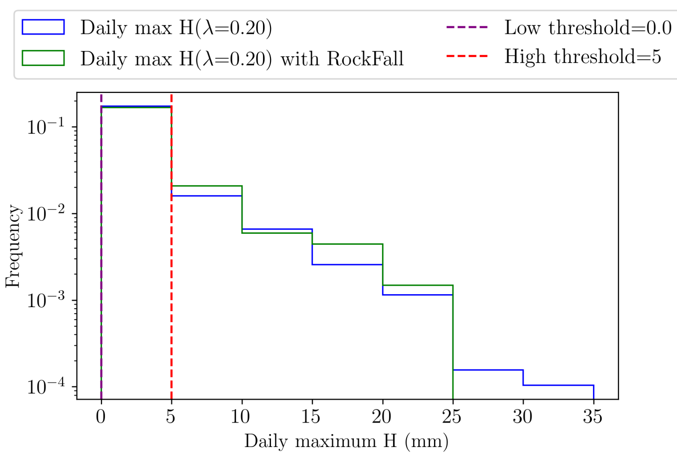

Figure 25. Distribution of H for $\lambda = 0.2$.

https://doi.org/10.5194/egusphere-2026-3939
Preprint. Discussion started: 12 August 2026

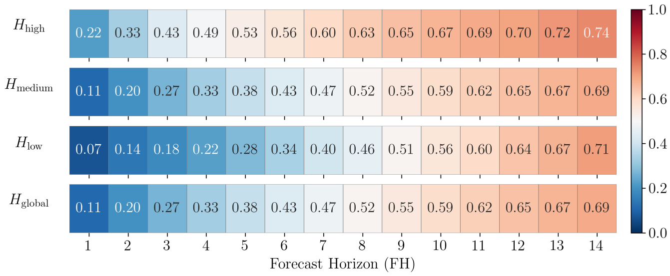

Figure 26. Heatmap of $\mathcal{P}(R = 1 \mid H = 1)$ for different levels of H for $\lambda = 0.2$. The sub-figures show (from the bottom to the top): the global probability H_{global} across all intensity levels, H_{low} intensity, H_{medium} intensity and H_{high} intensity.

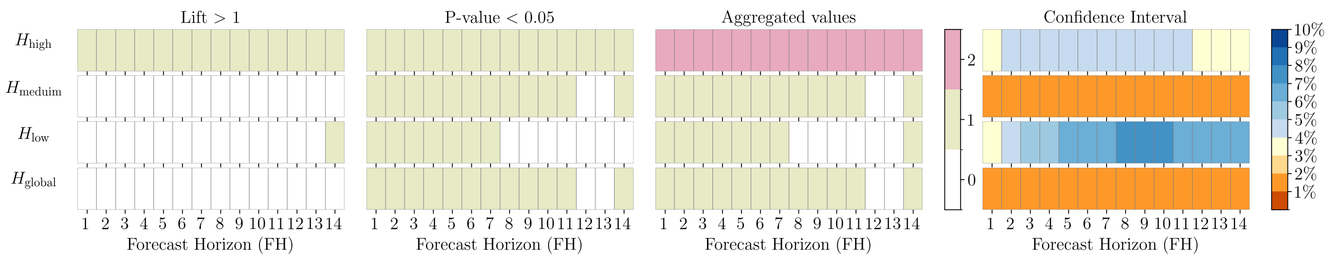

Figure 27. Results of metrics and aggregation for different levels of H for $\lambda = 0.2$, followed by the CI across varying thresholds. The sub-figures show (from the bottom to the top): the global aggregation H_{global} across all intensity levels, H_{low} intensity, H_{medium} intensity and H_{high} intensity.

However, growth with the forecast horizon is a reflection of both the physical process and the implicit effect of the more time we spend observing a phenomenon, the more likely we are to see it.

Figure 27 represents the metrics and aggregation results for different rainfall charge-discharge scenarios. This integrated analysis enables the identification of the forecast horizons for which rainfall storage provides the strongest and most reliable association with rockfall occurrence. For H_{global} case where we consider all samples of $H > 0$ regardless the intensity, the results show a statistical significance across nearly all forecast horizons with a low margin of error for CI. This suggests that the presence of charge-discharge event rainfall even without considering its intensity is associated with a rockfall occurrence.

Going further in detailed analysis by incorporating intensity levels. The result of high intensity charge H_{high} shows a strong statistical association to rockfall occurrence over all the forecast horizon (lift > 1 and p-value < 0.05) and the aggregated score reaches its maximum, reinforcing the effect of high intensity rainfall discharge on predicting the rockfall events. However, when analyzing the CI, it gives much higher uncertainties than other cases, and this is due to the smaller number of events occurring at high intensity levels. Conversely, H_{low} shows a much weaker effect. Indeed, it scores just one significant metrics on short forecast horizon, then it drops in significance to meet almost no metrics after day 7, and by looking at the CI larger uncertainties are observed in this level for longer forecast horizons. This indicates a low predictive strength and uncertainty

https://doi.org/10.5194/egusphere-2026-3939
Preprint. Discussion started: 12 August 2026

for low intensity charge. The H_{medium} case falls between the two by following a similar trend as the global charge showing a moderate significance.

This results demonstrate that ground saturation plays an important physical role in controlling rockfall occurrence.

3.3 Probability of Rockfall Conditioned on Temperature

To explore the relationship between temperature and rockfall activity, we analyze the probability of rockfall occurrence conditioned on the presence of freezing temperatures. We consider two scenarios in order to understand how negative temperature in terms of continuous freezing and freezing depth influences rockfall activity.

3.3.1 Continuous Freezing

We define the continuous freezing condition $T_f =$ as a period where at least one recorded temperature per day is below 0°C throughout the entire RH. As above in the previous analysis, RH and FH are set to 14. So, we computed the probability of rockfall under this condition ($M = T_f = 1$) to evaluate if freezing plays a role in triggering rockfalls, given by this formula:

$$\mathcal{P}(R=1 \mid T_f=1) = \frac{\mathcal{P}(R=1 \cap T_f=1)}{\mathcal{P}(T_f=1)} \tag{19}$$

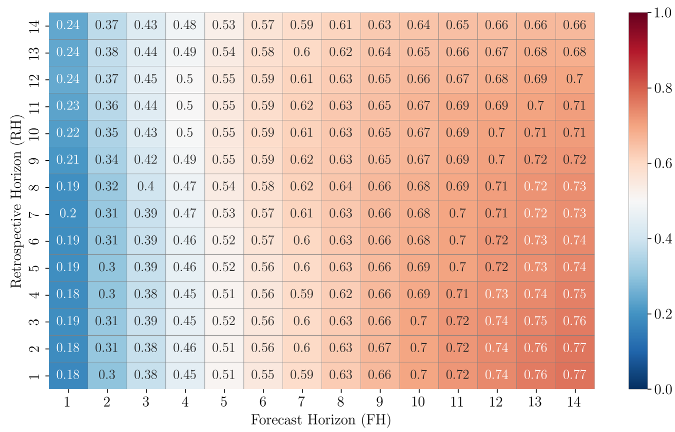

Figure 28. Heatmap of $\mathcal{P}(R=1 \mid T_f=1)$ as a function of RH and FH.

The results of $\mathcal{P}(R=1 \mid T_f=1)$ on heatmap 28 show that for a fixed RH, the probability of rockfall consistently increases with FH. We observe that from $FH = 8$, the probabilities are stabilized around 0.6-0.77. This behavior is expected because longer forecast horizons tend to have a greater number of potential rockfall occurrences, resulting in higher cumulative probabilities. And also this can suggest that the destabilizing effects of freezing are not immediate and this delayed effect may represents the time for thawing. However, the probability is relatively stable in most of cases or shows a slight effect as we increase RH.

https://doi.org/10.5194/egusphere-2026-3939
Preprint. Discussion started: 12 August 2026

Then we computed our metrics as followed in the methodology section to better evaluate temporal influence of continuous freezing conditions.

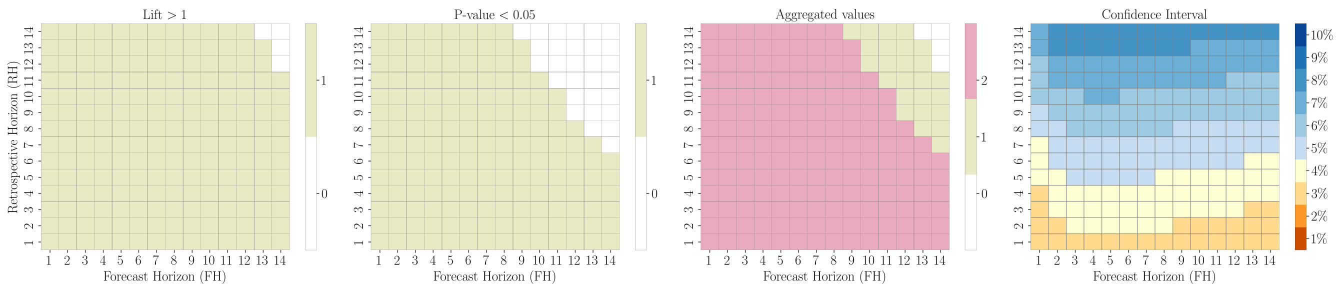

Figure 29. Metrics and aggregation results, followed by the CI across varying thresholds of continuous freezing $\mathcal{P}(R=1 \mid T_f=1)$ as a function of RH and FH.

As shown in Figure 29, we found that the entire heatmap of lift is almost filled with ones excepts for very large horizons, this suggests that continuous freezing condition always increase the likelihood of rockfalls compared to the baseline probability of rockfall. For the p-value of test χ^2, almost all horizons show a statistical significance between freezing temperature and rockfalls. However, the confidence interval heatmap provides a complementary and essential perspective on these results. It shows a clear trend where each decrease of uncertainty is associated with a progressive reduction of the significant horizon RH. This reduction is associated with a decrease at the beginning up to 2 days in the FH horizon. The significance of the retrospective horizon progressively decreases as we focus on lower uncertainty levels, but the forecast horizon remains stable. This reinforces the idea that long retrospective horizons (prolonged period of freezing) does not affect rockfalls and the effect is less significant. So, freezing contributes to rock weakens but its impact on rockfall is more significant and stronger for continuous freezing periods around (RH : 1-8 days) and all forecast horizon FH : 1-14 days.

3.3.2 Freeze depth

In order to better understand the contribution of temperature to rockfall triggering, we introduce a simple model to estimate the temperature at depth, based on the one-dimensional heat diffusion equation. The model does not account for heat exchange due to water phase transition (freezing and thaw), neither solar radiation. We consider only conduction in the rock and air temperature applied on the free surface.

$$\frac{\partial u(x,t)}{\partial t} = \alpha \frac{\partial^2 u(x,t)}{\partial x^2} \tag{20}$$

α being the thermal diffusivity, that can be expressed a function of thermal conductivity, λ_{th}, specific heat capacity, C and density, ρ :

$$\alpha = \frac{\lambda_{th}}{\rho C} \tag{21}$$

https://doi.org/10.5194/egusphere-2026-3939
Preprint. Discussion started: 12 August 2026

For the calcareous rock of the Saint Eynard cliff, common values for these properties are $\lambda_{th} = 1.5\ W.m^{-1}.K^{-1}$, $C = 800\ J.kg^{-1}.K^{-1}$, $\rho = 2500\ kg.m^{-3}$ what gives $\alpha = 7.510^{-7}\ m^2.s^{-1}$

We solved this equation using finite-difference method with an explicit scheme, considering semi-infinite medium for which the air temperature is applied on one side corresponding to the free surface. The depth is discretized by N nodes between x=0 and x=2 m with spacing of Δx. Time is discretized with spacing of Δt by successively solving the system, each solution in time providing temperature at each node in depth. Next equation shows the numerical scheme in which u_i^n stands for temperature at depth node i and time step n

$$u_i^{n+1} = u_i^n + \alpha \frac{\Delta t}{\Delta x^2}\left(u_{i+1}^n - 2u_i^n + u_{i-1}^n\right) \tag{22}$$

Stability condition imposes that $\alpha \frac{\Delta t}{\Delta x^2} \leq \frac{1}{2}$. In our case, Δt is set 1 hour to correspond to the time sampling of the measured temperature, what impose $\Delta x \geq 0.073\ m$. We set $\Delta x = 0.08\ m$.

We solve the equation at each time step by iterating over the node i, imposing $u_0^{n+1} = T_0$, T_0 being the measured temperature of the air at the considered time step and $u_N^{n+1} = T_D$, T_D being the temperature at depth. Here we considered T_D equals the average temperature over the whole period of measurement.

Once solved, the model allows to estimate the depth to which freezing temperatures penetrate the rock mass. At each time step, the freeze depth D_f is determined as the deepest point where temperature drops below 0°C. For our analysis study, these hourly estimates are aggregated at the daily scale by simply retaining for each the day the maximum value of D_f which represents the deepest freezing reached on that day.

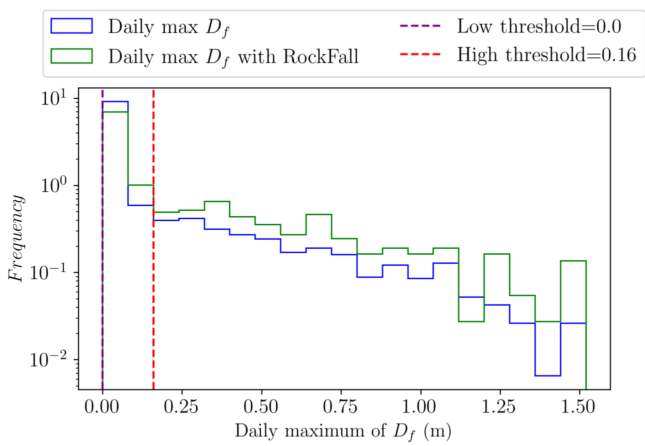

Figure 30. Distribution of maximum D_f.

We redefine M in our probability as follow: $M = D_f$, we define three levels of freeze depth D_f based on how deeply freezing temperatures penetrate during a day:

- $\mathbf{D_{f,Global}}$: where $D_f > 0$. This level captures all instances where freezing occurs, regardless of how it is shallow or deep.

https://doi.org/10.5194/egusphere-2026-3939
Preprint. Discussion started: 12 August 2026

- $\mathbf{D_{f,High}}$: this level happens when, the maximum freezing depth during the day reaches or exceeds 0.16 m, based on over-representation of maximum freeze depth values associated with rockfalls) as illustrated on Figure 30. Here cold temperatures are penetrating enough into the rock.
- $\mathbf{D_{f,Low}}$: when the maximum freeze depth during the day remains below 0.16 m, but is not zero. In this case, the freezing is limited to the surface.

Then we calculate the probability of rockfall on the following days of FH given freeze depth for each level.

$$\mathcal{P}(R=1 \mid D_{f,level}=1) = \frac{\mathcal{P}(R=1 \cap D_{f,level}=1)}{\mathcal{P}(D_{f,level}=1)} \tag{23}$$

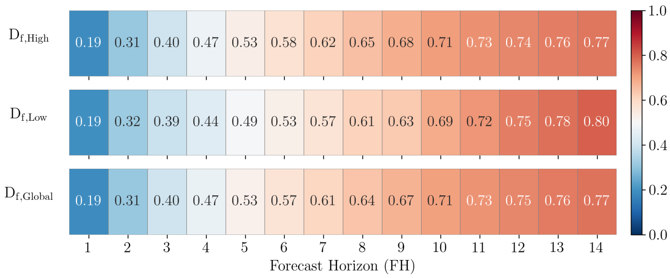

Figure 31. $\mathcal{P}(R=1 \mid D_{f,level}=1)$ for different depth levels of freeze D_f. From the bottom to the top : $D_{\text{f,Global}}$, $D_{\text{f,Low}}$ and $D_{\text{f,High}}$.

Figure 31 illustrates the results of conditional probability of rockfall occurrence given a depth freezing level over forecast horizons ranging from 1 to 14 days. It represents a clear trend showing that probabilities increase with increasing forecast horizon length. Indeed, all the depth levels show a convergence toward high probability (above 0.7) after a period of horizon from 10 to 14 days.

In the global case $D_{\text{f,Global}}$ which takes into account any freeze depth, the probability increases regularly. Focusing on the freeze depth levels. The $D_{\text{f,High}}$ results are closely mirrored to the global case. We can see also that $D_{\text{f,Low}}$ case despite representing slower freezing it shows a similarly increase in the probability with a slightly higher probabilities beyond 11 days.

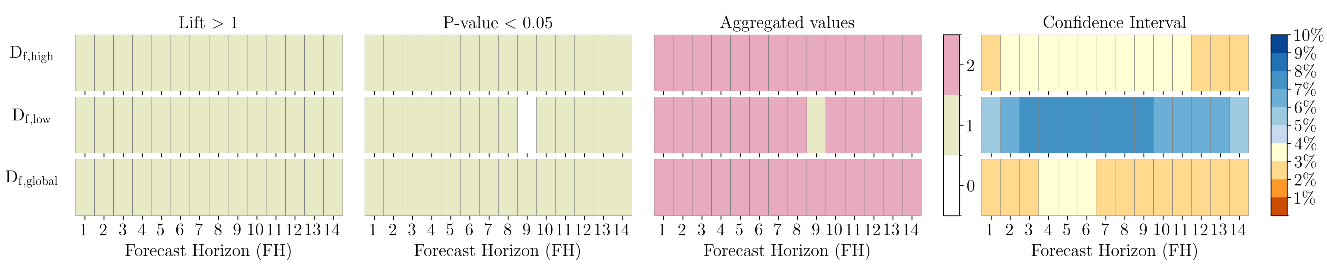

Figure 32. Metrics and aggregation results, followed by the confidence interval across multiple threshold level of different freeze depth D_f. From the bottom to the top : $D_{\text{f,Global}}$, $D_{\text{f,Low}}$ and $D_{\text{f,High}}$.

https://doi.org/10.5194/egusphere-2026-3939
Preprint. Discussion started: 12 August 2026

This increase is partly expected, as increasing the forecast horizon naturally increase the likelihood of observing at least one rockfall event. These results can highlight that while freeze depth matters, even shallow or high freezing, if it is persistent, can play an important role in rockfall triggering.

Then, we aggregated the binary results of the two metrics for each forecast horizon to identify which periods of time are strong and statistically significant, on Figure 32. $D_{\mathrm{f,Global}}$ shows a strong statistical significance across the entire forecast horizon FH which reflects that any freezing level is associated with elevated rockfall risk with low uncertainties of confidence interval. When differentiating by depth, we have clear distinctions. High freeze depth condition $D_{\mathrm{f,High}}$ maintains statistical significance across all horizons by achieving the maximum aggregated score, and with low confidence interval values which reflects more robust results. Therefore, $D_{\mathrm{f,Low}}$ presents a slight variability, while the lift and the p-value thresholds still significant and the aggregation give almost a maximum score, the confidence interval presents a high level of uncertainty, which can be expected when analysing rare events over the period, resulting in a lower reliability in the relationship for decision-making.

4 Discussion

The results of this study confirm that rainfall and freezing temperature play a significant role in rockfall triggering events at Mont Saint-Eynard.

Our analysis, shows that rockfalls are more likely to occur after a continuous rainfall lasting from 1–4 day duration. This aligns with the findings of Delonca et al. (2014) from La Reunion, where a cumulative 2-day rainfall (RH) with FH of 1 day led to a rockfall probability of 0.32 when rainfall intensity is between 15-20 mm and a probability of 0.55 when rainfall intensity is between 40-50 mm. And from Burgundy, where rockfalls are less frequent (the daily probability of rockfall is 0.02), a cumulative 3 days rainfall (RH) with a delay of 2 days FH lead to a rockfall probability of 0.04 when rainfall intensity is between 15-20mm.

Then, by categorizing rainfall into low and high intensities and rockfalls into small and large events, the results show (i) a weak and non-significant statistical association is observed between low intensity rainfall and the occurrence of large rockfall, (ii) a localized significance for short horizons $RH = 1-3$ and $FH = 1-6$ days indicating that low rainfall intensity can destabilize surface and cause small magnitude rockfall (iii) the occurrence of large rockfalls is mostly strongly associated with intense rainfall (>16.42 mm/day) particularly when it is on short retrospective horizon of 1-3 days (iiii) small rockfall have slightly significance response under heavy intensities of rainfall on short horizons ($RH = 2-3$ days and $FH = 1$ day).

So, these results indicate that high magnitude rockfalls are more sensitive to intense and recent rainfall. They align with the findings of Krautblatter and Moser (2009) where they underscore the importance of rainfall intensity as a triggering factor for rockfalls based on a four-year measurement in a high Alpine rock wall (Reintal, German Alps). In fact, continuous rainfall is a powerful trigger of rockfalls in general, but the intensity of rainfall is more significant in triggering large magnitude events.

For the charge-discharge rainfall analysis, it adds an important information by capturing the cumulative effect of precipitation over time, and the contribution of past rainfall decrease due to a decay parameter λ. This approach completes the method with fixed horizon RH, by giving a more flexible and physically representation based on the evolution of ground saturation. The

https://doi.org/10.5194/egusphere-2026-3939
Preprint. Discussion started: 12 August 2026

results show that the likelihood of rockfall occurrence increases regularly with higher charge, confirms the idea that cumulative water over time, even for moderate rainfall, contributes significantly to destabilization. This is coherent with findings of Nissen et al. (2022), who showed that a pore water proxy based on accumulated precipitation performs slightly better than soil moisture in triggering rockfall events.

In addition to the mechanisms based on rainfall, our analysis of freezing continuous condition reveal that even short duration of persistent freezing can significantly increase the probability of rockfalls occurrence especially when followed by longer forecast horizons (Probability > 0.7 for FH > 10 days) which is coherent with the findings of Nissen et al. (2022) that freeze–thaw cycles on the previous period of 9 days give the optimal information value IV which is used to rank the freeze-thaw according to the rockfall. The delayed effect may be caused by thawing processes, which lead to stress and a potential weakening of rock. However, as the retrospective horizon RH is more extended, the increase in rockfall probability diminishes which can indicate that prolonged freezing alone is not sufficient to maintain high levels of instability or lead to reduced thaw driven activity.

Incorporating freeze depth into the analysis brings a more realistic picture of how cold temperatures interact with rock. Our results of probability suggest that even shallow freezing (< 16 cm) can increase the likelihood of rockfalls, this aligns with a previous study on Haute-Gaspésie showing that winter freeze–thaw cycles influenced only the first 15 cm from the surface Birien and Gauthier (2023). But when freezing penetrates deeper into the rock (> 16 cm), the statistical link becomes much stronger. These results indicate that surface freezing itself regardless of depth can have a significant impact because it can block water cracks.

These results show the relevance of combining different metrics across a multi-period statistical methodology. While in previous study, rockfall events are manually recorded based on visual observation, not detected through seismic signals and they often rely on fixed period of analysis and conditional probability without looking to other important statistical dimensions to reinforce the analysis.

5 Conclusion and Perspectives

This study provides a detailed statistical analysis of the role of rainfall and freezing conditions in triggering rockfalls at Mont Saint-Eynard. By combining multiple meteorological descriptors including continuous rainfall, intensity based thresholds, charge–discharge models to represent cumulative effects of rain over time, as well as freezing duration and depth. Our results reveal that both precipitation intensity and freezing play a crucial role, highlighting the importance not only of the quantity and duration of rainfall, but also of its intensities.

Recent and high intensity rainfall are particularly associated with high-magnitude rockfalls, while smaller events can be triggered by moderate precipitation. And for cold temperature, even shallow freezing increases the likelihood of rockfalls, while deeper freeze penetration shows a more robust statistical link with triggering.

Although probabilistic approaches capture essential relationships, they are still limited to predefined thresholds and conditions. But, by revealing relationships on multiple horizons lengths through statistical measures, this study highlights important features to be taken into account in the use of eXplainable AI methods to identify hidden and complex patterns and guide the formulation of hypothesis for future rockfall prediction systems.

So further progress could involve using artificial intelligence (AI) models for rockfall forecasting to independently learn non-linear and more complex temporal patterns from different data, by training deep learning algorithms on meteorological time series and seismic event records. These models have the potential to detect dependencies or combinations of factors that are challenging to identify using traditional statistical methods. Coupling these models with eXplainable AI methods (XAI), will then make it possible to extract explainable patterns from the predictions, helping to build new hypothesis leading to rockfall from meteorological data. This will enable to deepen our understanding of triggering processes.

Code and data availability. The source code used for this study is available on GitHub: https://github.com/bouazizS/Impact-of-meteorological-conditions-on-rockfalls.The data used in this study can be accessed via the link in the repository's README file.

Author contributions. AH produced the seismic catalog, AH and DA produced the seismic data, SB and DA performed the analysis, SB wrote the manuscript, and all authors interpreted the results and revised the manuscript.

Competing interests. The authors declare that they have no competing interests.

Acknowledgements. This research was funded by the French National Research Agency (ANR) under the project C2R-IA (https://anrc2ria.fr/), grant ANR-22-CE56-0005-06.

https://doi.org/10.5194/egusphere-2026-3939
Preprint. Discussion started: 12 August 2026

References

Allen, R. V.: Automatic earthquake recognition and timing from single traces, Bull. Seismol. Soc. Am., 68, 1521–1532, https://doi.org/10.1785/BSSA0680051521, 1978.

Birien, T. and Gauthier, F.: Assessing the relationship between weather conditions and rockfall using terrestrial laser scanning to improve risk management, Natural Hazards and Earth System Sciences, 23, 343–360, 2023.

Bourke, P.: Cross correlation, Cross Correlation", Auto Correlation—2D Pattern Identification, 596, 1996.

Chanut, M.-A., Lévy, C., Meignan, L., Gasc, M., Trouvé, E., Atto, A., Meger, N., Courteille, H., de Barros-Santos, G. C., and Nancy, G.: Démonstrateur d'utilisation de l'Intelligence Artificielle pour la gestion opérationnelle des risques naturels gravitaires géologiques Projet RINA, 2021.

Chanut, M.-A., Courteille, H., Lévy, C., Atto, A., Meignan, L., Trouvé, E., and Gasc-Barbier, M.: Managing Rockfall Hazard on Strategic Linear Stakes: How Can Machine Learning Help to Better Predict Periods of Increased Rockfall Activity?, Sustainability, 16, 3802, 2024.

Clauset, A., Shalizi, C. R., and Newman, M. E. J.: Power-Law Distributions in Empirical Data, SIAM Review, 51, 661, https://doi.org/10.1137/070710111, 2009.

Coron, C.: Outil 22. Le test du chi-deux, BàO La Boîte à Outils, pp. 74–77, 2020.

Craparo, R. M.: Significance level, Encyclopedia of measurement and statistics, 3, 889–891, 2007.

D'Amato, J., Hantz, D., Guerin, A., Jaboyedoff, M., Baillet, L., and Mariscal, A.: Influence of meteorological factors on rockfall occurrence in a middle mountain limestone cliff, Natural Hazards and Earth System Sciences, 16, 719–735, 2016.

Delonca, A., Gunzburger, Y., and Verdel, T.: Statistical correlation between meteorological and rockfall databases, Natural Hazards and Earth System Sciences, 14, 1953–1964, https://doi.org/10.5194/nhess-14-1953-2014, 2014.

Dussauge, C., Grasso, J. R., and Helmstetter, A.: Statistical analysis of rock fall volume distributions: implications for rock fall dynamics, Journal of Geophysical Research, B 108, 2286, DOI : 10.1029/2001JB000 650, 2003.

D'Amato, J.: Apport d'une base de données d'éboulements rocheux obtenue par scanner laser dans la caractérisation des conditions de rupture et processus associés, Bulletin of Engineering Geology and the Environment, 78, 653–668, https://doi.org/10.1007/s10064-017-1032-5, 2017.

El Mazouri, F. Z., Abounaima, M. C., and Zenkouar, K.: Data mining combined to the multicriteria decision analysis for the improvement of road safety: case of France, Journal of Big Data, 6, 1–30, 2019.

Graber, A. and Santi, P.: Power law models for rockfall frequency-magnitude distributions: review and identification of factors that influence the scaling exponent, Geomorphology, 418, 108 463, https://doi.org/10.1016/j.geomorph.2022.108463, 2022.

Guerin, A., Hantz, D., Rossetti, J.-P., and Jaboyedoff, M.: Brief communication "Estimating rockfall frequency in a mountain limestone cliff using terrestrial laser scanner", https://doi.org/10.5194/nhessd-2-123-2014, 2014.

Helmstetter, A. and Garambois, S.: Seismic monitoring of Séchilienne rockslide (French Alps): Analysis of seismic signals and their correlation with rainfalls, Journal of Geophysical Research: Earth Surface, 115, 2010.

Krautblatter, M. and Moser, M.: A nonlinear model coupling rockfall and rainfall intensity based on a four year measurement in a high Alpine rock wall (Reintal, German Alps), Natural Hazards and Earth System Sciences, 9, 1425–1432, 2009.

Le Roy, G., Helmstetter, A., Amitrano, D., Guyoton, F., and Le Roux-Mallouf, R.: Seismic Analysis of the Detachment and Impact Phases of a Rockfall and Application for Estimating Rockfall Volume and Free-Fall Height, Journal of Geophysical Research: Earth Surface, 124, 2602–2622, https://doi.org/10.1029/2019jf004999, 2019.

https://doi.org/10.5194/egusphere-2026-3939
Preprint. Discussion started: 12 August 2026

Nissen, K. M., Rupp, S., Kreuzer, T. M., Guse, B., Damm, B., and Ulbrich, U.: Quantification of meteorological conditions for rockfall triggers in Germany, Natural Hazards and Earth System Sciences, 22, 2117–2130, 2022.

Olivier, M.: Statistiques inférentielles-2e édition, Ellipses Marketing, 2024.

Provost, F., Malet, J.-P., Hibert, C., Helmstetter, A., Radiguet, M., Amitrano, D., Langet, N., Larose, E., Abancó, C., Hürlimann, M., Lebourg, T., Levy, C., Le Roy, G., Ulrich, P., Vidal, M., and Vial, B.: Towards a standard typology of endogenous landslide seismic sources, Earth Surface Dynamics, 6, 1059–1088, https://doi.org/10.5194/esurf-6-1059-2018, publisher: Copernicus GmbH, 2018.

Rat, M.: Optimisation de la gestion de la route du littoral à la Réunion vis-à-vis du risque de chutes de blocs, Bulletin des laboratoires des Ponts et Chaussées, 2006.

Tseng, M.-C. and Lin, W.-Y.: Efficient mining of generalized association rules with non-uniform minimum support, Data & Knowledge Engineering, 62, 41–64, 2007.

Vallet, A.: Mouvements de fluides et processus de déstabilisation des versants alpins : Apport de l'étude de l'instabilité de Séchilienne, Theses, Université de Franche-Comté, https://theses.hal.science/tel-01340359, 2014.